DEPARTMENT OF THE INTERIOR
U.S. GEOLOGICAL SURVEY

Subsurface structure of the Silsilah Ring Complex, as deduced from telluric-electric and audio-magnetotelluric investigation, Kingdom of Saudi Arabia

by

Charles J. Zablocki[1/], Edward A. du Bray[2/], Carl L. Long[2/], and Charles L. Tippens[2/]

Open-File Report 85-238

Prepared for the Ministry of Petroleum and Mineral Resources, Deputy Ministry for Mineral Resources, Jiddah, Kingdom of Saudi Arabia

This report is preliminary and has not been reviewed for conformity with U.S. Geological Survey editorial standards and stratigraphic nomenclature.

1/ U.S. Geological Survey Saudi Mission
2/ U.S. Geological Survey, Denver, CO

1985

CONTENTS

ILLUSTRATIONS

SUBSURFACE STRUCTURE OF THE SILSILAH RING COMPLEX AS DEDUCED FROM TELLURIC-ELECTRIC AND AUDIO-MAGNETOTELLURIC INVESTIGATIONS, KINGDOM OF SAUDI ARABIA

by

Charles J. Zablocki[1], Edward A. du Bray[2], Carl L. Long[2], and Charles L. Tippens[2]

ABSTRACT

An electrically conductive zone, delineated by the telluric-electric profiling technique, is located on the western side of the Silsilah ring complex and is interpreted to be intensely argillically altered, potentially mineralized rock. The top and bottom of this conductive zone are at depths of about 150m and 400m, respectively.

Geoelectric cross sections (contoured values of resistivity as a function of depth) constructed from audio-magnetotelluric data obtained at 2- to 3-km intervals over the entire complex show a broad, high-resistivity zone located in the central part of the complex that probably reflects the dense, inner core of a shallow pluton. A low-resistivity zone is peripheral to this feature. Resistivities of the rocks in the peripheral zone are generally much higher than those characteristic of the western zone of exceptionally low- resistivity. Peripheral zone resistivities are distinctively lower, however, than those in the central area or those associated with the ring structure. The average width and depth of this zone exceeds a kilometer and may represent a volume of weakly clay-altered rock concentric about the hypothesized core pluton. Several telluric-electric profiles made across the complex corroborate the audio-magnetotelluric findings.

INTRODUCTION

Subproject 5.12.11 was established in 1403/04 AH within the work program of the Deputy Ministry for Mineral Resources to develop and apply the telluric-electric (TE) profiling and audio-magnetotelluric (AMT) geophysical methods as part of the U.S. Geological Survey (USGS) mineral resource assessment program. The present study was initiated because favorable results were obtained during feasibility studies of these methods in several parts of the Jabal Hibshi quadrangle (Flanigan and Zablocki, 1984). Large electrical-property contrasts among the major rock types encountered demonstrated the utility of these

1/ U.S. Geological Survey Saudi Mission
2/ U.S. Geological Survey, Denver, CO

sub-regional scale, electromagnetic techniques for reconnaissance mapping of the geoelectric structure to depths exceeding a kilometer.

Subsequent TE and AMT surveys were largely extensions and follow-up investigations of previously studied areas. They include the Meshaheed district (Smith and Samater, 1984), the Silsilah ring complex (du Bray, 1985), and portions of the Raha fault zone (du Bray, *in press*). In addition, measurements were made with the AMT system at several sites on the Paleozoic cover rocks near Buraydah to determine the depth to crystalline basement. Most of these studies were made using equipment and data reduction facilities on loan from the Geophysics Branch of the USGS in Denver, Colorado. An AMT system is being designed and fabricated in Denver and will soon be available for use in the Saudi Arabian Mission. This should facilitate acquisition of data in economically or structurally important areas.

Not all of the data acquired in the 1404 AH field surveys have been reduced because the availability of the reduction system (desk-top computer and digitizer) in Denver has been limited. The bulk of the data that has been reduced was collected as part of a study of the Silsilah ring complex. In this report we discuss the results of an analysis of these data and present a generalized geologic model of the ring complex based on reasonable geologic assumptions that are compatible with the geoelectric results.

ACKNOWLEDGMENTS

The work on which this report is based was performed in accordance with an agreement between the Saudi Arabian Ministry of Petroleum and Mineral Resources and the USGS. This report has benefited from technical review of an earlier version by Robert Kamilli.

GEOLOGY OF THE SILSILAH RING COMPLEX

The circular ring complex is centered at lat 26°07'N. and long 42°42'E., about 150 km west-southwest of Buraydah (fig. 1), near the northeastern limit of the Arabian Shield. The geology, petrogenesis, and mineral resource potential of the Silsilah ring complex is discussed in detail by du Bray (1985). The complex is an igneous suite, mostly composed of highly evolved rocks, that crops out in a ring fracture, and, to a much lesser extent, inside the ring fracture (fig. 2). A core pluton is hypothesized to be present in the shallow subsurface at the center of the complex. A U-Pb zircon age for the Fawwarah alkali-feldspar granite, the youngest component of the ring complex, is 587 ± 8 Ma (J.S. Stacey written communication, 1984). The composition and plutonic characteristics of the rocks that compose the Silsilah ring complex are similar to those of other plutons exposed in the northeastern Arabian Shield that were emplaced

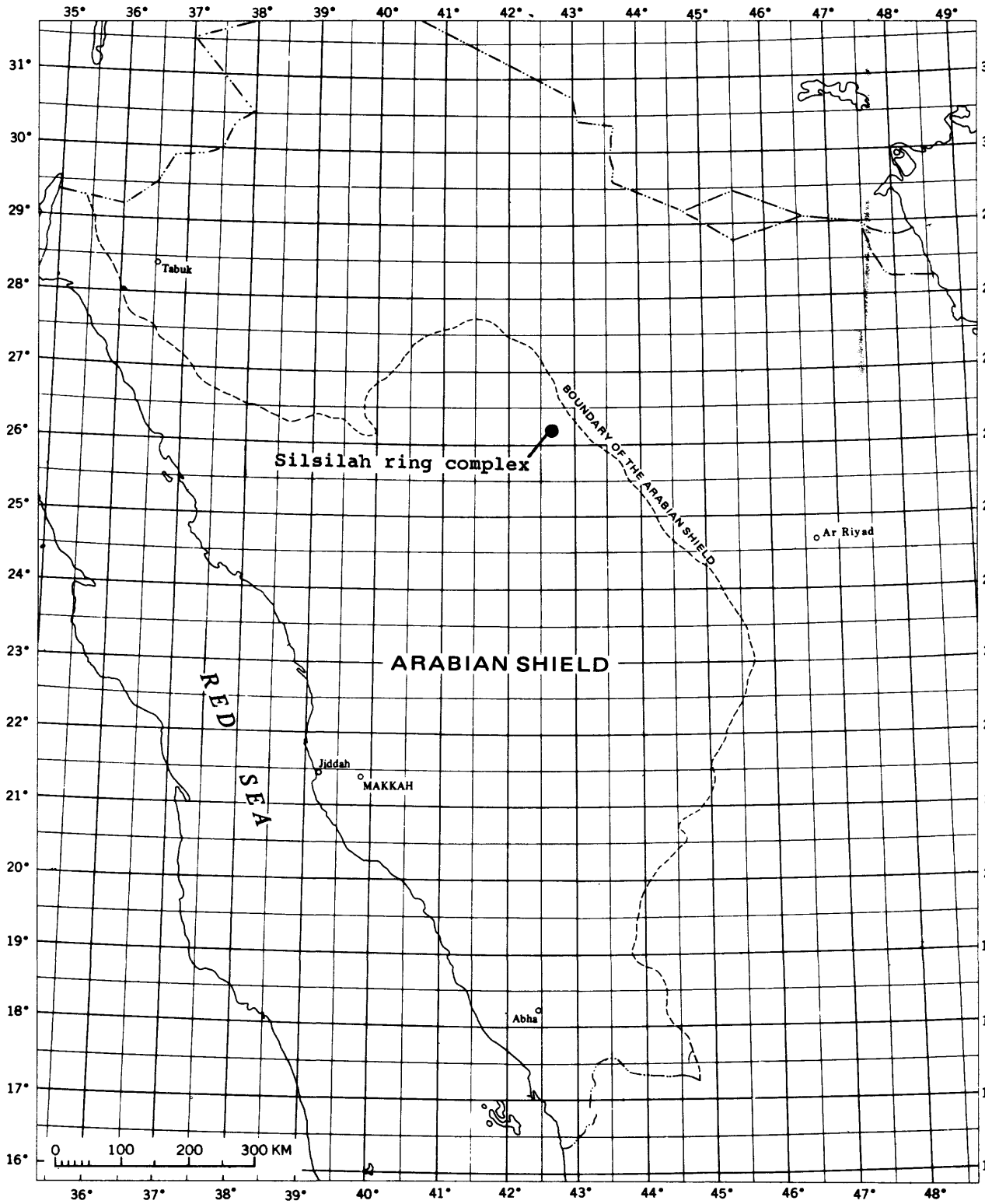

Figure 1.--Index map of western Saudi Arabia showing the location of the Silsilah ring complex.

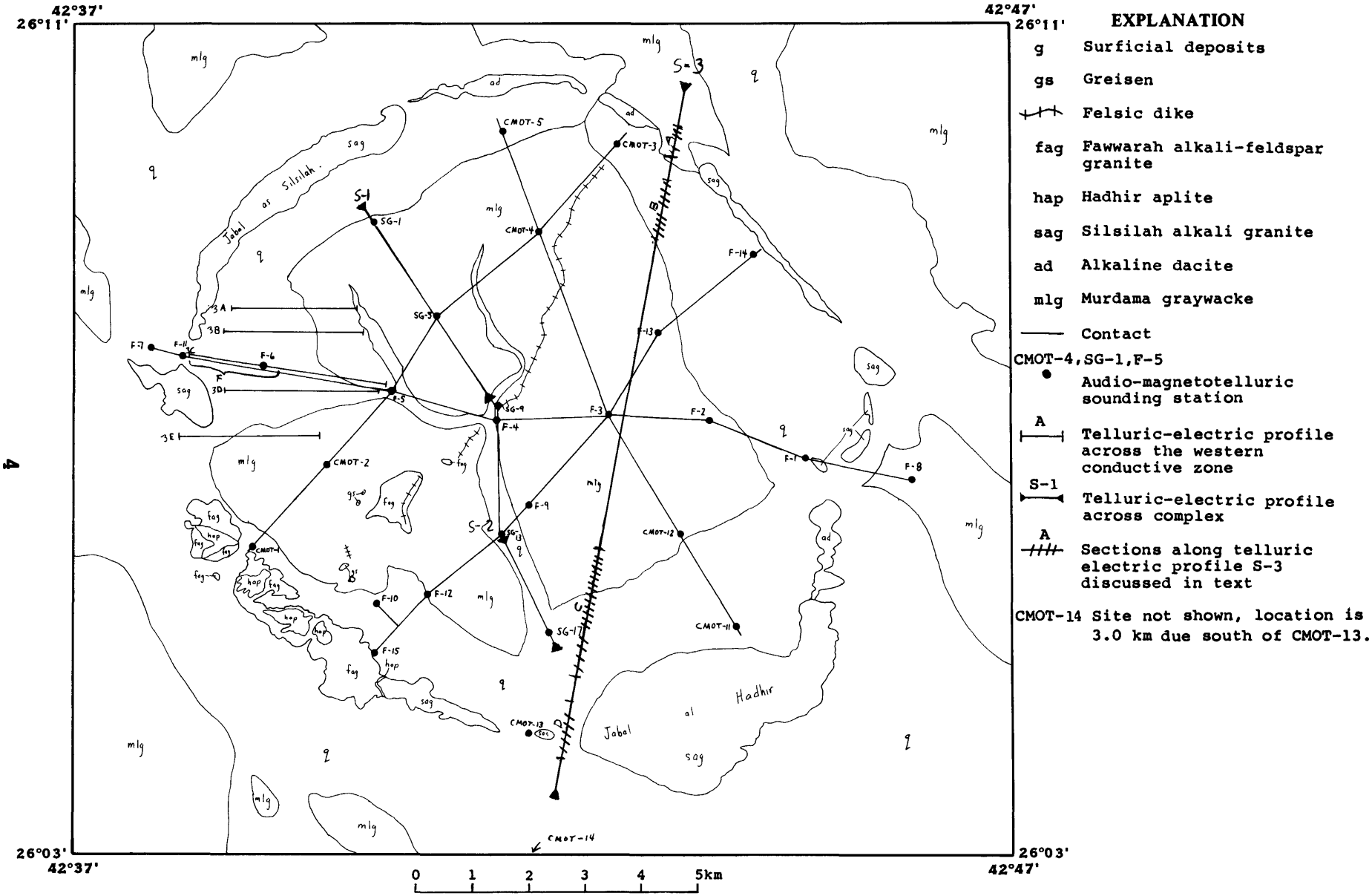

Figure 2.--Simplified 1:50,000-scale geologic map of the Silsilah ring complex showing the location of geoelectric traverses.

between 570 and 580 Ma ago (Stuckless and others, 1984). Rocks of the ring complex intrude graywacke sandstone of the Murdama group; the sandstone crops out within the ring complex and occurs in a large area outside the ring.

The rocks exposed in the ring complex form a prominent toroidal topographic feature that is 12 km in diameter and rises between 10 and 300 m above the surrounding pediment surface; the average relief along the ring is about 100 m. The cross-sectional area of the toroidal feature is between 50 m in the northeast and about 2.5 km in the southeast. Rock exposed in the ring may represent magma that was confined to a zone of closely spaced ring fractures.

Three principal and several minor igneous rock types form the ring complex. The northwest and southeast quadrants are largely composed of Silsilah alkali granite, the southwest quadrant is predominantly Fawwarah alkali-feldspar granite, and the Hadhir aplite forms a carapace that overlies the alkali-feldspar granite. These intrusive rocks account for about 40, 20, and 10 percent of the ring complex, respectively. Two other rock types crop out in the east and northeast quadrants. One is very fine grained alkaline rock, composed of mugearite, benmoreite, trachyte, and tristanite, as defined by Irvine and Baragar (1971). These are alkaline analogs of dacite and are referred to as alkaline dacite. The second type is fine-grained, porphyritic comendite and is chemically equivalent to the Silsilah alkali-granite. Both lithologies are characterized by textures that suggest quenching. Very coarse grained quartz-potassium feldspar pegmatite occurs throughout the aplite but is most abundant in a zone between the Fawwarah alkali-feldspar granite and the Hadhir aplite. Quartz veins cut the granite and aplite. Two intensely mineralized greisens that locally contain high-grade accumulations of cassiterite are located less than 0.5 km inside the southern part of the ring. Weakly mineralized greisens occur at several places inside the southwest part of the ring and several more occur within the ring itself.

TECHNIQUES

Telluric-electric method

The source of most of the telluric-electric (TE) measurements collected in this study was natural micropulsation electromagnetic energy centered around a 30-second period (0.033 Hz). A comprehensive description of the theory and techniques of this method has been presented by Flanigan and Zablocki (1984). Basically, the TE method utilizes telluric (earth) currents that owe their origin to sunspot activity. The voltages developed by these currents between two pairs of grounded electrodes are measured along linear traverses that may extend for tens of kilometers. From the measurement of the relative ratio of the

resulting electric fields, a profile is constructed that reflects the gross electrical characteristics of the underlying rocks. In addition to utilizing micropulsations as an electromagnetic field source, several studies were made in which the electric fields produced from spherics (distant lightning discharges in the lower atmosphere) were measured in the frequency range between 7.5 and 75 Hz. Here, shorter (50 m) length bipole spacings were used instead of the longer (250 or 500 m) length bipoles that were used with the 0.033 Hz source. This modified telluric profiling technique, using higher and multiple frequencies and shorter-length bipole separations allows for mapping the boundaries of shallow conductive zones in more detail and also provides relative, uncalibrated depth information of these zones.

Audio-magnetotelluric method

Relevant aspects of the AMT method have also been described by Flanigan and Zablocki (1984). The electromagnetic signals from spherics are measured at discrete frequencies between 4.5 Hz and 7.5 KHz with a high-sensitivity, selectively-tuned receiver that is connected to appropriate electric and magnetic sensors. Electromagnetic signals of higher frequencies, to 27 KHz, are also measured using man-made transmitters as sources. From the ratio of the horizontal, orthogonal components of the electric and magnetic fields at a given frequency, the apparent resistivity of the earth can be determined. Because the depth to which electromagnetic waves travel in the earth is dependent on their frequency (high frequencies-shallow; low frequencies-deep), the AMT method provides a means of sensing the resistivity distribution as a function of depth by making measurements over several decades of frequency. AMT stations are usually sited at 2- to 3-km intervals. The reduced data are usually presented as geoelectric cross sections or in plan view in which the resistivity distribution is displayed in contour form.

When using the scalar AMT system, the resistivities are generally computed from the log average of measurements made in both a N-S and E-W direction. In an electrically isotropic medium (horizontally layered), the computed resistivities at a given frequency will be identical. Where lateral changes in resistivity occur within the sensing range of the electromagnetic fields, the computed resistivities will differ in the two directions. A more sophisticated system (tensor) measures all the parameters of the electric and magnetic fields and can, in many situations, define two- or three-dimensional features in greater detail. Also, the inversion process that is used in generating geoelectric models assumes a horizontally layered earth. Therefore, the AMT results should be viewed as a first-order approximation of the actual geoelectric substructures that provides very useful information concerning the gross electrical characteristics of the ring complex to depths in excess of a kilometer.

RESULTS AND DISCUSSION

Western electrically conductive zone

A mass of very low-resistivity rock approximately 1 km in diameter located at a shallow depth near the western interior of the ring complex was identified by measurements made during the feasibility study (Flanigan and Zablocki, 1984). This low-resistivity zone might be related to intensely altered or fractured rock, and confirmation of this possibility might be achieved by defining the lateral extent and configuration of the zone.

During the follow-up study of the ring complex, five subparallel traverses (designated 3a through 3e) were made across the feature using the TE profiling technique at 0.033 Hz (fig. 2). The initial traverse (3c), established along a portion of the traverse that was made during the feasibility study, consisted of 250-m-long bipoles instead of the earlier 500-m-long bipoles for better resolution of the feature. The resulting profile (fig. 3c), defined the general shape of the anomaly in greater detail than its predecessor. The relative E-field amplitudes decrease by a factor of 50 to 1 from the west end of the traverse to the central part of the conductive zone located about 1 km east of the ring complex. For a two-dimensional vertical contact, such a ratio would correspond to a resistivity ratio of 2500 to 1 (see equation 3 in Flanigan and Zablocki, 1984). The subsequent traverses showed, however, that the feature does not have a large enough lateral extent to approximate a two-dimensional structure and, therefore, the resistivity ratio may be smaller. An AMT sounding made over a portion of this feature during the feasibility study indicated that the conductive zone has a minimum resistivity of about 15 ohm-m, and that the part of the ring complex exposed to the west has a resistivity of several thousand ohm-meters (Flanigan and Zablocki, 1984). It is likely that the actual resistivity of the most conductive part of the zone is less than 15 ohm-m, since the sounding interpretation assumes horizontal layering of infinite lateral extent.

Four additional TE profiles served to outline the general configuration of the zone (fig. 3a, b, d, and e). North of profile 3c, large and abrupt increases in the E-field amplitudes, along profiles 3a and 3b, clearly define the eastern boundary of the zone. The boundary at the western end of the zone was not defined along these traverses because the western-most electrode was located about 150 m east of the base of the exposed ring complex. This boundary probably lies somewhere between the base and the western-most electrode. Profile 3d indicated that the width of the most conductive part of the zone narrows considerably from that in the area of profile 3c. Also, the shallower increase in the E-field gradient on the east side of

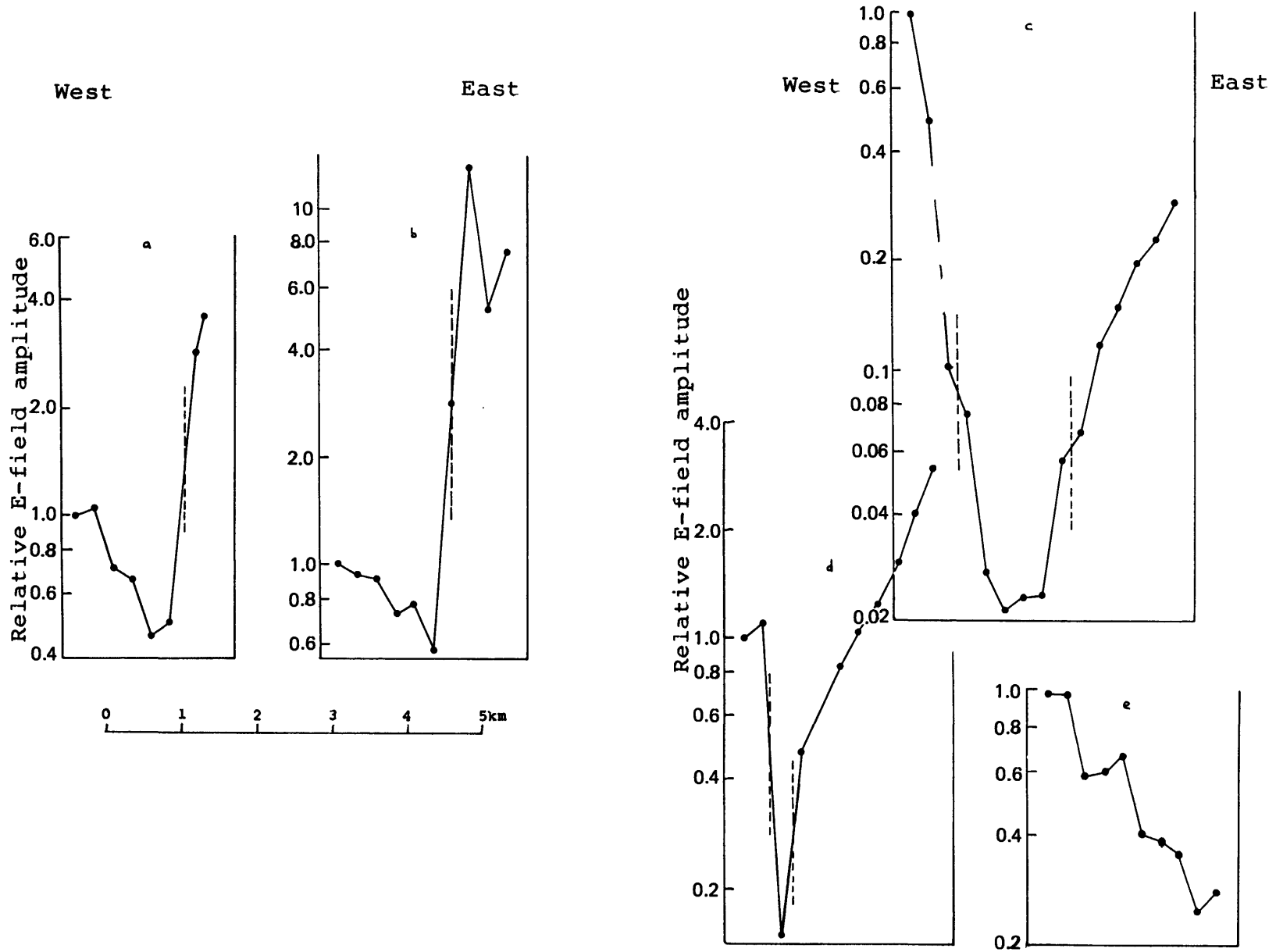

Figure 3a-e.--Telluric-electric profiles across the conductive zone on the west side of the complex. Profiles 3a-e correspond to 3a-e, respectively, on figure 2. Dashed vertical lines on profiles a and b coincide with the east edge of the conductive zone whereas dashed vertical lines on profiles c and d define both sides of the zone.

both profiles 3c and 3d suggests a correspondingly gradual increase in the resistivity to the east, and contrasts with the abrupt change in the vicinity of profiles 3a and 3b. The results of a traverse located about 1 km south of profile 3d (profile 3e) do not indicate any sharp conductive boundaries. The gradual decrease in the E-field amplitudes to the east may reflect responses from high resistivity, exposed and near-surface igneous rocks at the western end to moderately resistive metasedimentary rocks toward the eastern end of the profile.

The approximate limits of the most conductive part of this zone were established (vertical dashed lines on profiles 3a-d) and a plan view of the configuration of this zone was produced (fig. 4) with the results from these five traverses. The boundaries of the zone were not defined on the north side of profile 3a because data from a traverse in this area include an abnormally large time-phase shift in the observed E-field that probably results from an abrupt discontinuity in the resistivities at the edge of a near-parallel (east-west) boundary. This phenomenon was discussed by Flanigan and Zablocki (1984).

An experimental, telluric-electric profile was made along a portion of profile 3c to assess the utility of the aforementioned multifrequency-telluric profiling technique because of the large resistivity contrast of the rocks in this area. E-field ratios of natural spherics at 7.5, 27, and 75 Hz were measured at 50-m intervals over a distance of 1.7 km. The resulting profiles of the relative voltages provide additional insight into the geoelectric character of the underlying rocks (fig. 5). The steep gradient in all of these profiles near station 7 corresponds to the discontinuity noted in profile 3c and may reflect the contact between the igneous and metasedimentary rocks.

Dispersion in the relative voltages observed at these three frequencies becomes apparent in data collected between stations 11 and 16 and a larger separation is noted in the lower frequencies (7.5 and 27 Hz) eastward to the end of the profile. The depth of penetration of electromagnetic waves is inversely proportional to the square root of frequency in a uniformly conductive medium. Accordingly, the lowest frequency measured here (7.5 Hz) senses to depths approximately two and three times deeper than at 27 and 75 Hz, respectively. Therefore, the large differences in the relative voltages measured at these three frequencies can be qualitatively interpreted as resulting from decreasing rock resistivity with depth. In contrast to the 50 to 1 decrease observed along profile 3c at 0.033 Hz, the decrease is four times larger (200 to 1) at 7.5 Hz. This would imply that the conductive zone is underlain by rocks of higher resistivity. Data for the AMT sounding made in this area during the feasibility study (sounding F-6 in Flanigan and Zablocki, 1984)

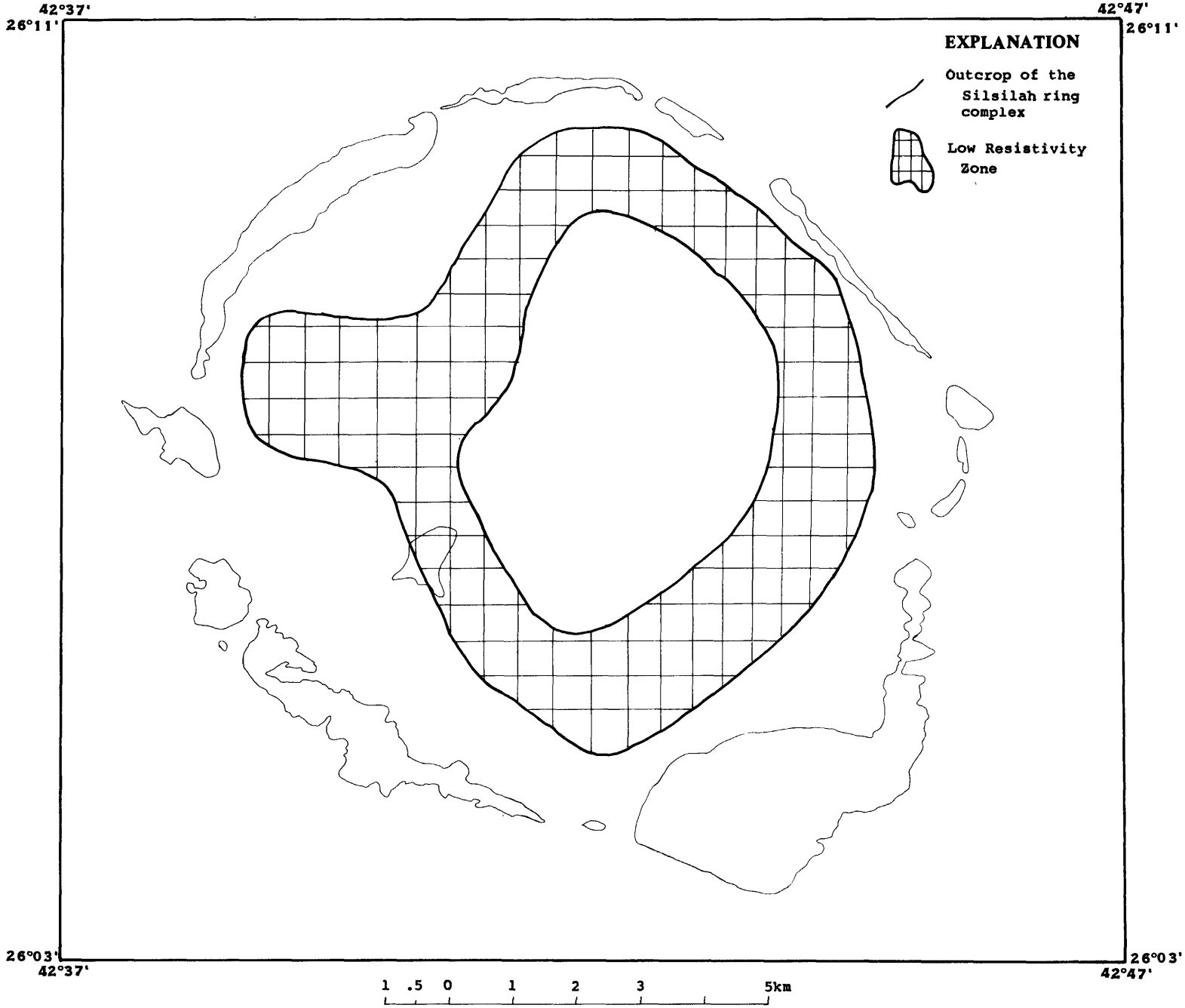

Figure 4.--Map showing the location of low resistivity zones (hachured) associated with the Silsilah ring complex.

Figure 5.--Multi-frequency telluric-eletric voltages along profile 3c (fig. 2). Station spacing is 50 m.

suggest that the top and bottom of the conductive zone are about 150 m and 400 m, respectively, below the surface.

The foregoing results facilitate speculation on the probable nature of this anomalous zone. First, the general configuration and restricted size of the zone does not appear to have resulted from tectonic processes such as sheering, faulting, or ring fracturing. These processes would produce linear or concordant patterns aligned with the exposed structures in the area. Further, in areas where the metasedimentary rocks are exposed over the feature, there is no evidence of unusual fracturing or shearing at the surface. Nor is it likely that a steeply dipping fracture zone would terminate at a shallow depth coincident with the inferred top of the conductive zone. Finally, it is unlikely that an increase in water-filled porosity, caused by percolation of water into fractures with a tectonic origin, could account for rock resistivities as low as 15 ohm-m or less. These low resistivities most probably indicate the presence of an abundant quantity of clay minerals. Clay minerals possess large cation-exchange capacities that cause the ion concentration available for conduction through the pore fluids to increase (Keller and Frischknecht, 1966, p. 24). This conductive feature probably results from a zone, up to several kilometers wide and several hundred meters thick, of intensely argillically altered rock.

Trenches 1 to 5 m deep excavated across the greisens in the southwest part of the ring complex indicate the association of intensely clay-altered rock with greisenized rock. The exsolution of a volatile-rich hydrothermal fluid from the alkali-feldspar granite melt during the waning stages of its solidification facilitated greisenization, and locally intense tin mineralization (du Bray, 1985). Away from the center of the hydrothermal system, the low-temperature conversion of granite and its host graywacke to an assemblage of clay minerals was achieved. One might infer from these observations that the possible clay alteration associated with the conductive zone is like that associated with the greisens. That is, the conductive zone may be associated with rock that is intensely mineralized like that currently exposed in the greisens. The presence of a quartz vein system (du Bray, 1985) cutting the Silsilah alkali-granite at the south end of Jabal as Silsilah, 1 km west of the conductive zone, provides further evidence that this area may have been the locus of an intense hydrothermal system. Unexposed rock associated with the conductive zone may be strongly mineralized.

Geoelectric structure of entire complex

In addition to the TE studies made over the shallow conductive feature, 13 AMT soundings and three 500-m spacing TE profiles were made to supplement the feasibility-study sounding

data. The AMT sites were nominally spaced at 2- to 3-km intervals so that the geoelectric structure of the entire complex could be characterized on a sub-regional scale (fig. 2). From the reduced AMT sounding curves, five geoelectric cross sections were constructed (figs. 6-10). The cross sections shown in figures 6 and 7 show a broad high-resistivity zone located in the central part of the complex. This feature probably reflects the dense inner core of a shallow pluton. A zone of low resistivity is peripheral to this feature. The resistivities of the rocks in the other parts of the peripherial zone are generally much higher than resistivities in the western zone. They are distinctively lower, however, than those in the central area or those coincident with the outer ring complex itself.

The other cross sections (figs. 8-10) indicate the same general pattern wherein a zone of low resistivity flanks the central area (fig. 4). The average width and depth of the peripheral zone exceeds a kilometer. The results from the 500-m-spaced TE profiles made across several parts of the complex corroborate the AMT findings (fig. 11). Low E-field amplitudes, corresponding to sections of relatively low resistivity, were measured in the vicinity of SG-5 along profile S-1, to the southeast of SG-13 along profile S-2, and in the areas identified as B and C along profile S-3. The long north-south TE profile (S-3) that was made across and through the complex also indicates the zones of relatively high resistivity associated with the ring dikes (labeled A and D), as well as the zone of high resistivity across the central part of the complex.

Compositional changes in the outer zone of a pluton could not cause the observed resistivity differences. The size and general configuration of the peripheral zone suggest that it could be related to concentric fractures that formed during the emplacement of the core pluton. The average resistivities are sufficiently low that they may be accounted for by an increase in fracture porosity. However, the surface rocks, like those exposed above the western conductive zone, appear to be undeformed and show no evidence of concentric fracturing.

Alternatively, the peripheral zone may represent a volume of weakly clay-altered rock concentric about the hypothesized core pluton. Shallow emplacement of such a pluton could have promoted exsolution of a late-stage fluid phase that may in turn have reacted with and altered previously solidified rock. The intensity of the proposed clay alteration is probably not great, because the observed resistivities are generally much greater than those determined for the western conductive zone.

Plan sections of the resistivity distribution at 500- and 1000-m depths (figs. 12 and 13) were derived from the two-dimensional cross sections. These sections provide another perspective of the geoelectric character of the complex. As

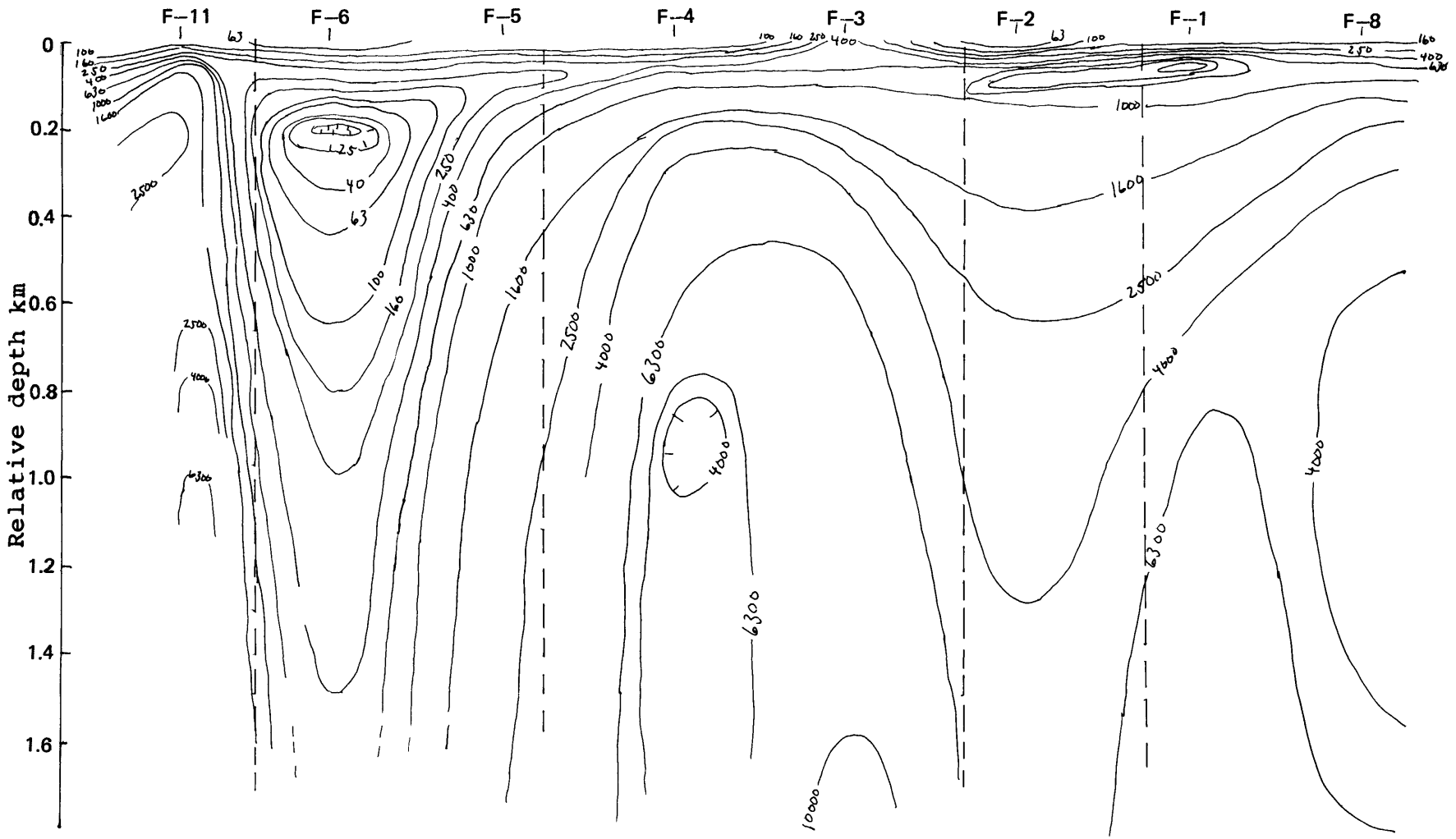

Figure 6.--Geoelectric cross section, derived from AMT measurements, along profile shown in figure 2. F-11 designates AMT station location. Logarithmically- spaced resistivity contours in ohm-m.

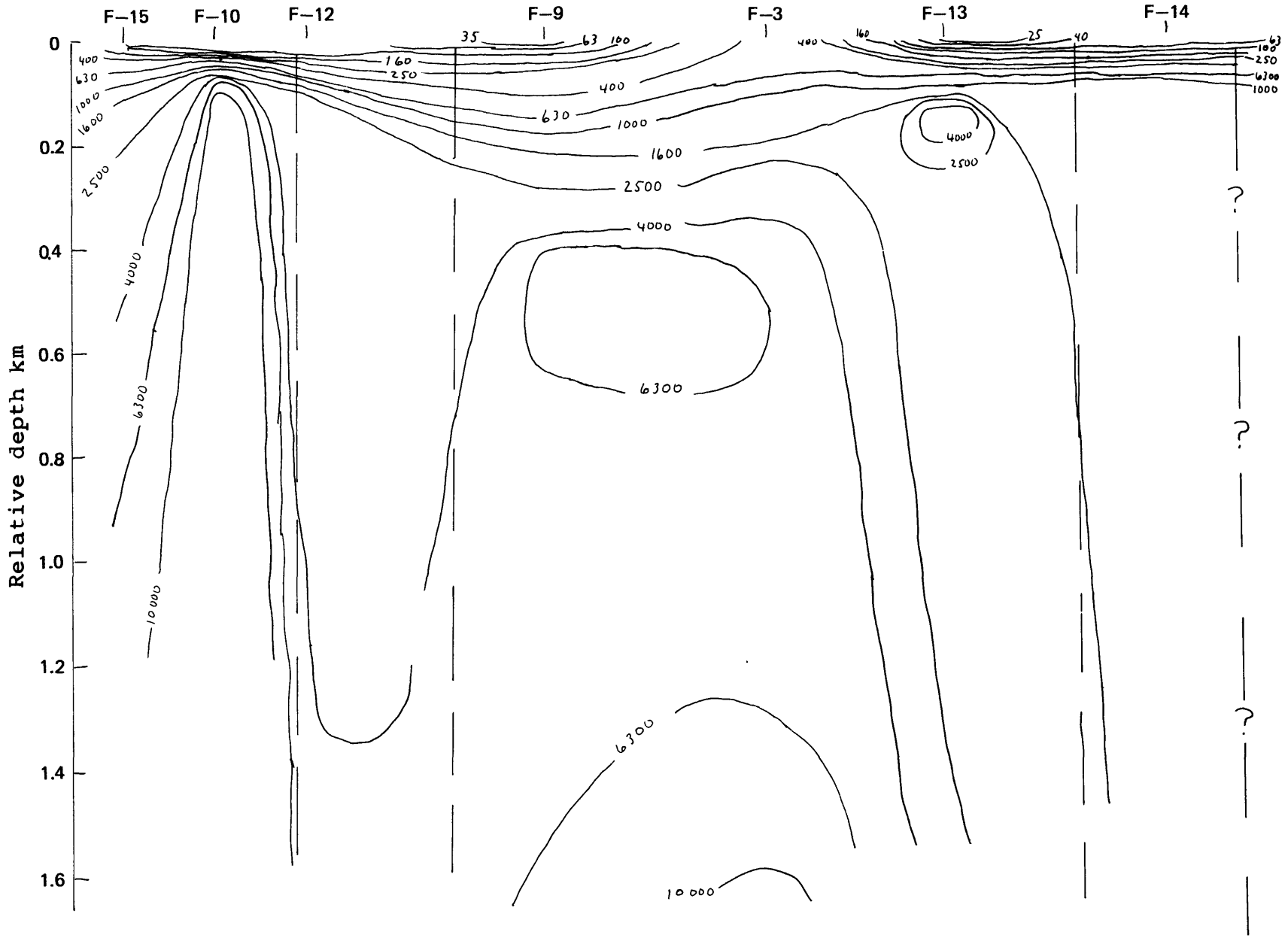

Figure 7.--Geoelectric cross section, derived from AMT measurements, along profile shown in figure 2. F-15 designates AMT station location. Logarithmically-spaced resistivity contours in ohm-m.

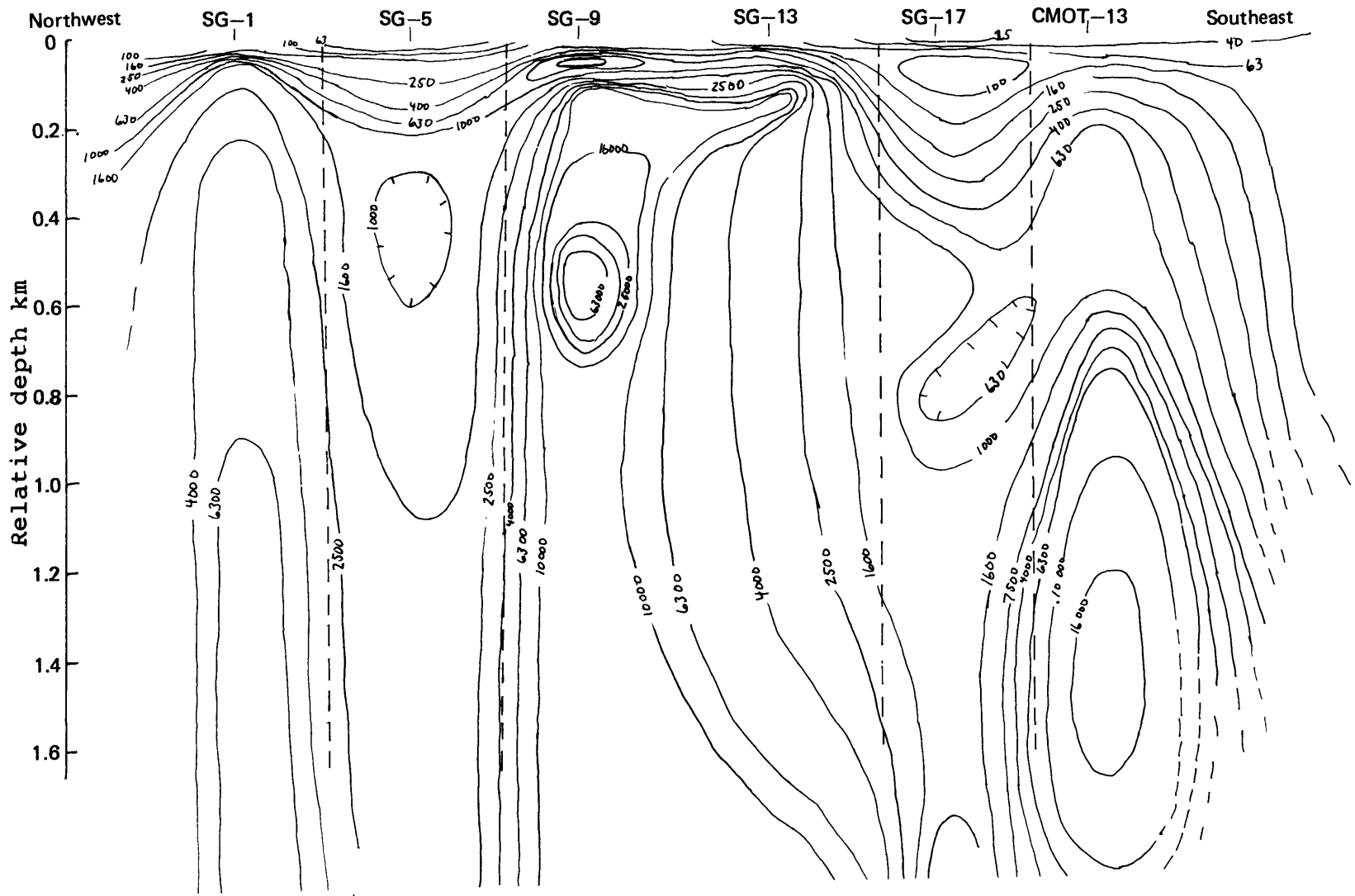

Figure 8.--Geoelectric cross section, derived from AMT measurements, along profile shown in figure 2. SG-1 designates AMT station location. Logarithmically- spaced resistivity contours in ohm-m.

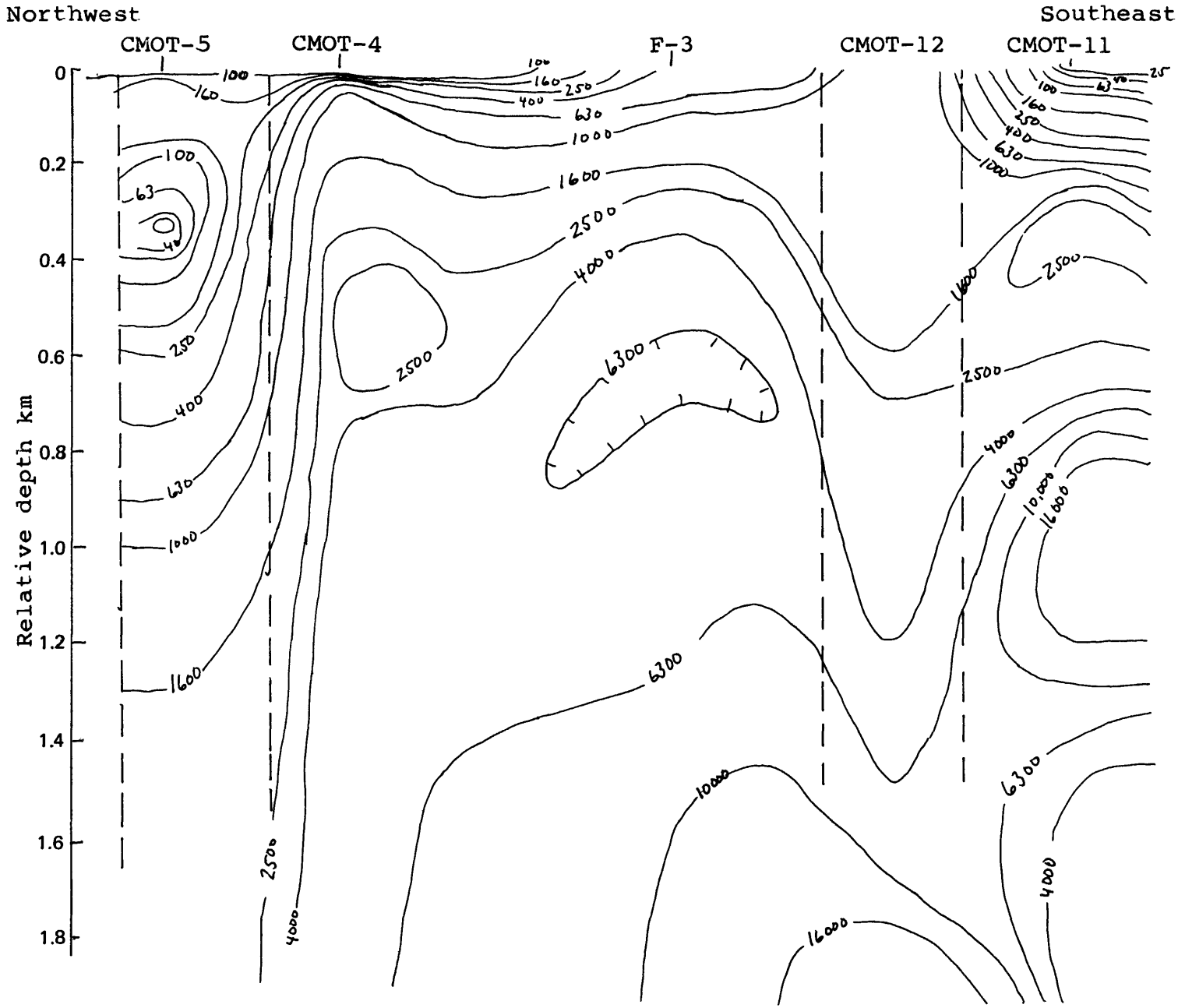

Figure 9.--Geoelectric cross section, derived from AMT measurements, along profile shown in figure 2. CMOT-5 designates AMT station location. Logarithmically- spaced resistivity contours in ohm-m.

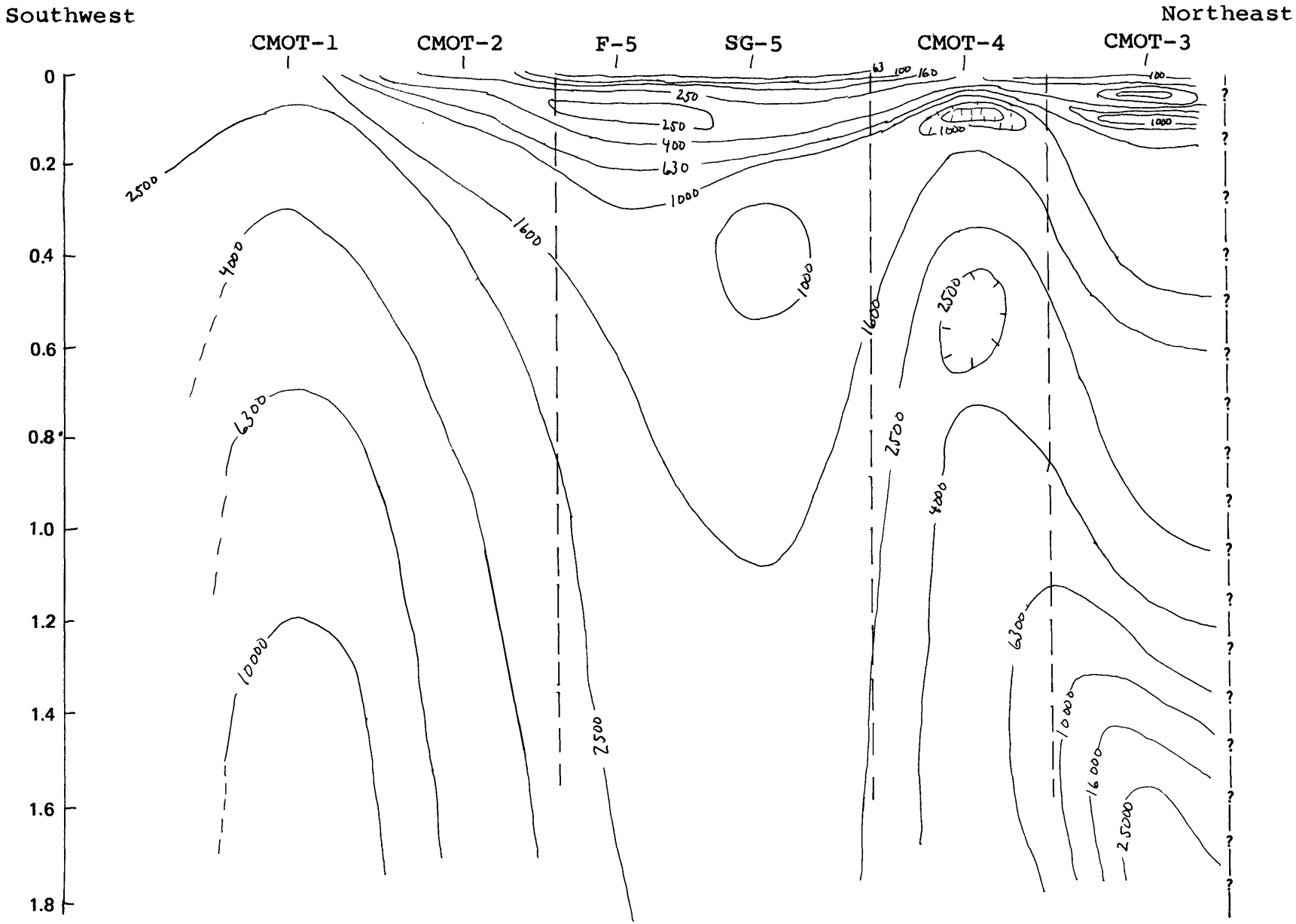

Figure 10.--Geoelectric cross section, derived from AMT measurements, along profile shown in figure 2. CMOT-1 designates AMT station location. Logarithmically- spaced resistivity contours in ohm-m.

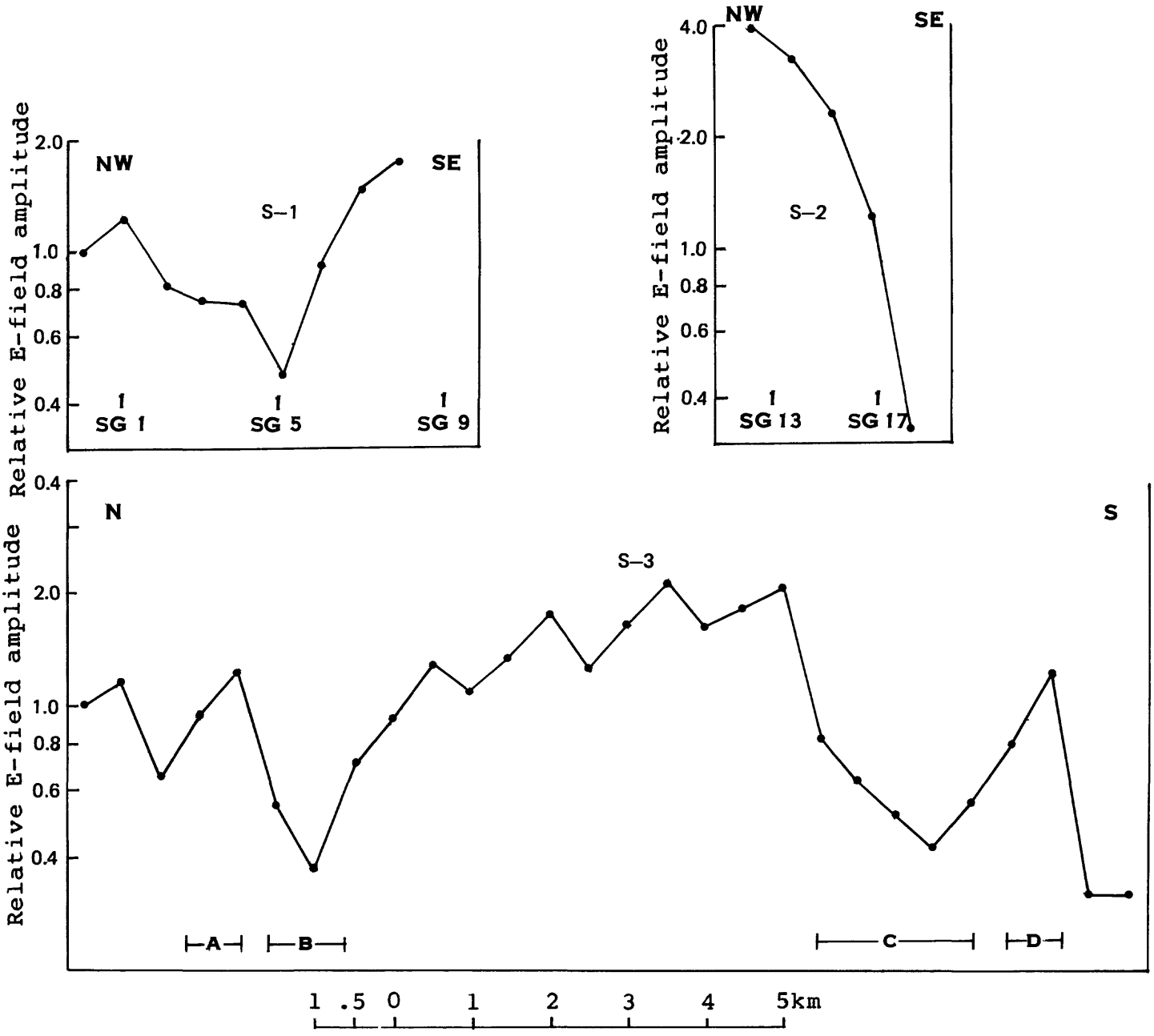

Figure 11.--Telluric-electric profiles shown in figure 2. SG-1 designates AMT station location.

these sections were produced by interpolation of data over rather large distances, they should not be interpreted too rigorously. The peripheral zone suggested from the cross sections is not clearly seen in these plan sections. This is in part due to the fact that the actual values of resistivity in this zone vary over a large range. A low-resistivity zone around the western high-conductivity zone appears to trend eastward for several kilometers. This was also suggested by the shallow gradient of the E-field amplitudes toward the east end of TE profiles 3c and 3d and from the results of the 500-m spacing TE profile made along the traverse through AMT stations SG-1 to SG-9 (S-1, fig. 11).

Other conductive zones are noted on the north and south sides of the complex. Neither are as conductive as the western high-conductivity zone. The one on the south side is particularly interesting because of its large size and closer proximity to the cassiterite-bearing greisens to the west. The results from the TE profiles S-2 and S-3 across this area indicate that the low-resistivity zone is fairly broad (fig. 11).

CONCLUSIONS AND RECOMMENDATIONS

The results from these natural-source-field electromagnetic surveys have demonstrated the utility of these methods in providing important insights into the gross substructure of the Silsilah ring complex. The electrical responses may be indicating the relative degree of argillic alteration that these rocks have undergone. This is so because of the large influence that clay minerals have on rock resistivity, particularly for igneous and metamorphic rocks such as those found here. In contrast, the influence of clay minerals in higher porosity, sedimentary rocks is usually smaller because of the dominance of electrolytic conduction through abundant water-filled interstices. Because mineralization is commonly associated with intense argillic alteration, the anomalously conductive features reported herein are worthy of follow-up investigations. These investigations should be focused initially toward determining the cause of these conductive zones. Although detailed geophysical surveys might provide further, but indirect, evidence for the existence of a low-temperature hydrothermal system, drilling is recommended at the central part of the western feature to provide unequivocal evidence. Drill data could then form the basis for consideration of continued studies at Silsilah as well as provide control for the interpretation of future electrical studies in similar settings elsewhere in the Kingdom. They could also contribute toward developing and refining conceptual ore-occurrence models that would have extrapolative value in other areas.

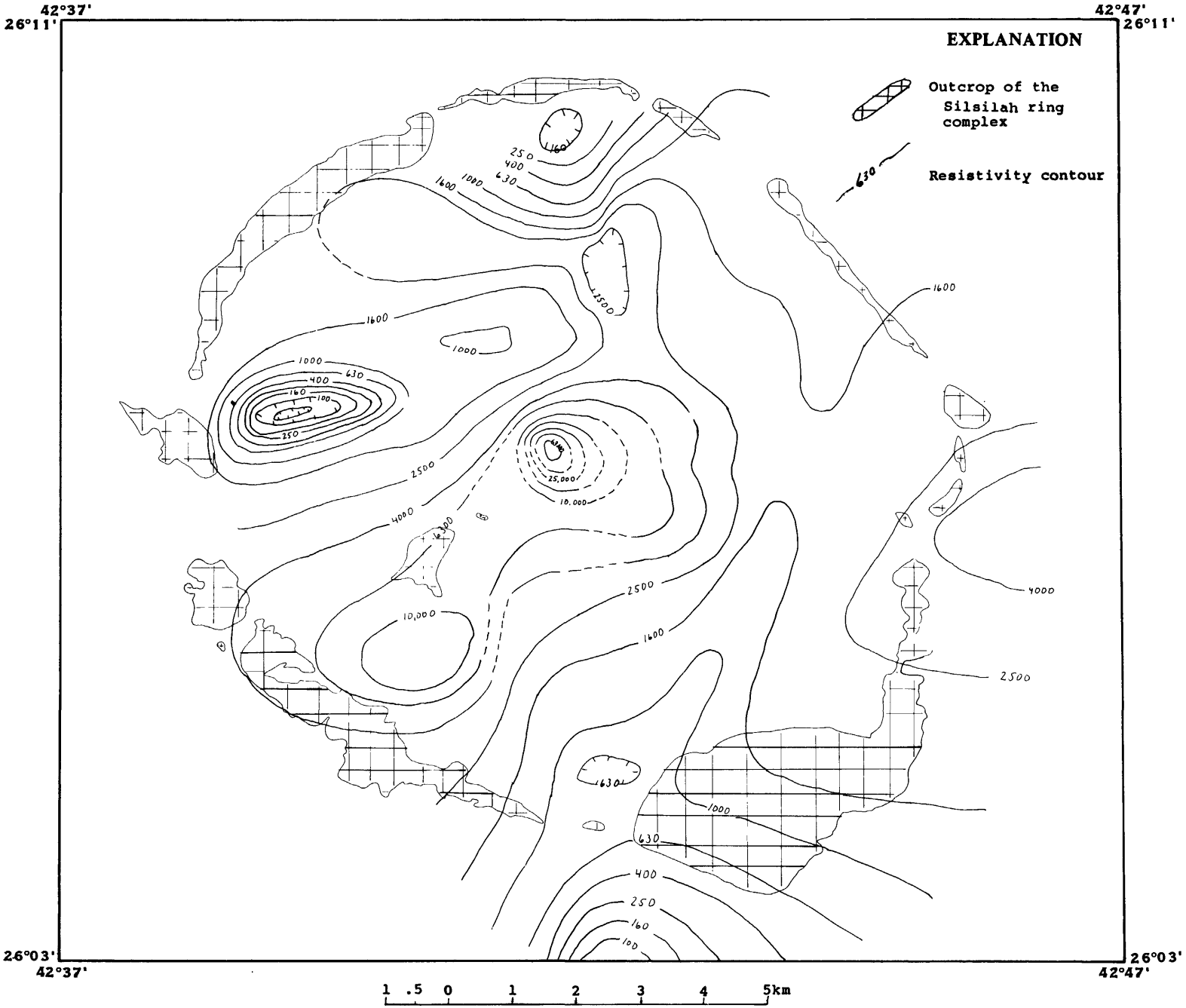

Figure 12.--Resistivity distribution map at a depth of 500 m below the surface.

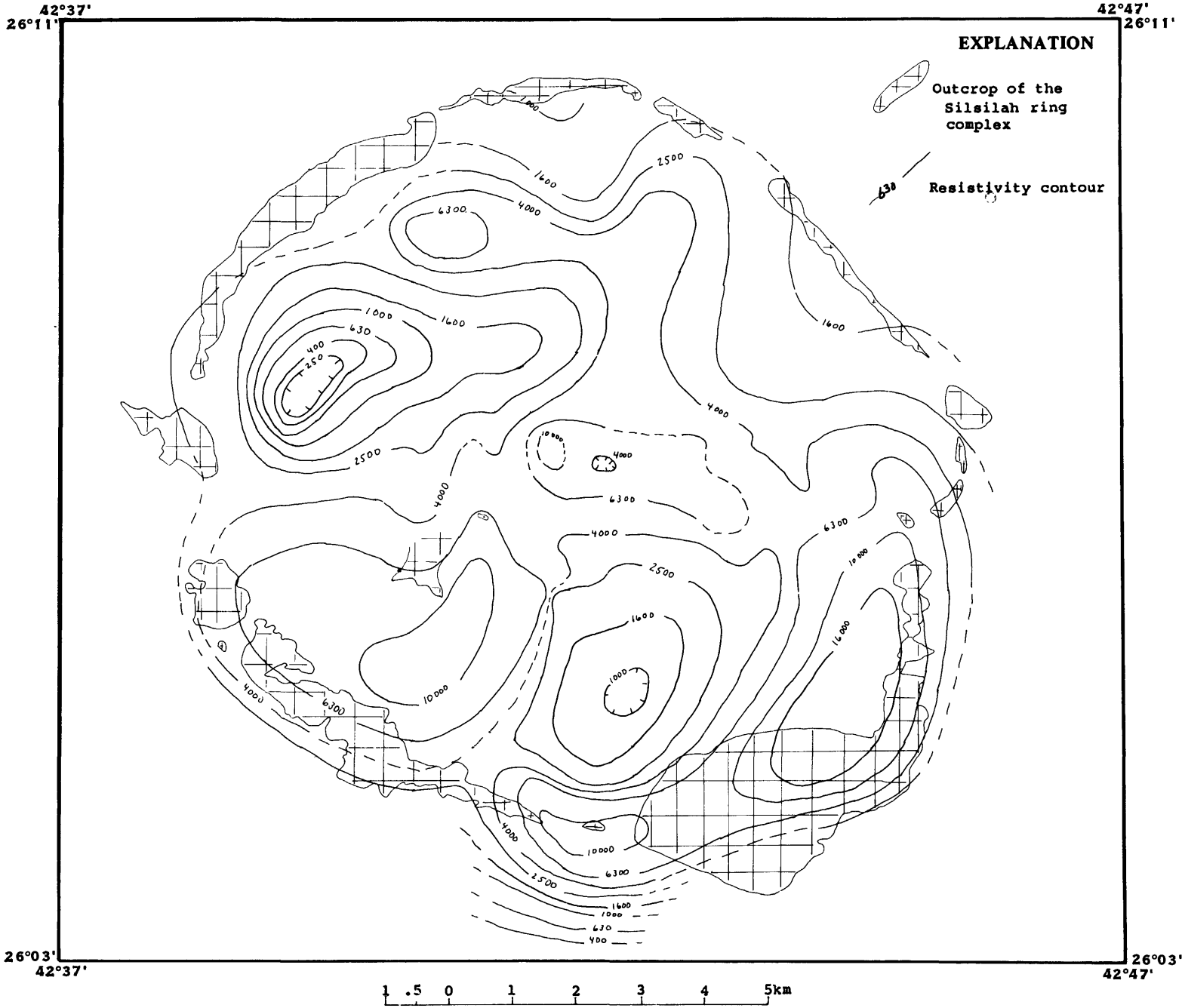

Figure 13.--Resistivity distribution map at a depth of 1000 m below the surface.

A secondary drilling target would be over the broad conductive feature toward the south end of the complex. Impetus for drilling in this area might come from any favorable results found from the studies of the western conductive feature. Here, however, it is recommended that some further electrical surveys be made initially for better definition of the configuration of this feature.

DATA STORAGE

Data file USGS-OF-5-46 (Zablocki and others, 1984) has been established for the storage of data used in this report.

No entries or updates have been made to the Mineral Occurrence Documentation System (MODS) data bank.

REFERENCES CITED

du Bray, E.A., *in press*, Reconnaissance geology of the Jabal as Silsilah quadrangle, sheet 26/42 D, Kingdom of Saudi Arabia: Saudi Arabian Deputy Ministry for Mineral Resources map series, 52 p., scale 1:100,000.

du Bray, E.A., (1985), Geology of the Silsilah ring complex, Kingdom of Saudi Arabia: U.S. Geological Survey Open-File Report 85-253.

Flanigan, V.J., and Zablocki, C.J., 1984, An evaluation of the applicability of the telluric-electric and audio- magneto-telluric methods to mineral assessment on the Arabian Shield: Saudi Arabian Deputy Ministry for Mineral Resources Open-File Report USGS-OF-04-26, 61 p.; also, 1984, U.S. Geological Survey Open-File Report 84-425.

Irvine, T.N., and Baragar, W.R.A., 1971, A guide to the chemical classification of the common volcanic rocks: Canadian Journal of Earth Sciences, v. 8, p. 523-548.

Keller G.V., and Frischnecht, F.C., 1966, Electrical methods in geophysical prospecting: Pergamon Press, New York, 517 p.

Smith, C.W. and Samater, R.M., (1984), Preliminary report on the gold deposits at Meshaheed, Kingdom of Saudi Arabia: Saudi Arabian Deputy Ministry for Mineral Resources Open-File Report USGS-OF-04-29, 38 p.; also, 1985, U.S. Geological Survey Open-File Report 85-9.

Stuckless, J.S., Hedge, C.E., Wenner, D.B., and Nkomo, I.T., *in press*, Isotopic studies of postorogenic granites from the northeastern Arabian Shield: Contributions to Mineralogy and Petrology.

Zablocki. C.J., du Bray, E.A., Long, C.L., and Tippens, C.L., 1984, Supporting data for the subsurface structure of the Silsilah ring complex from telluric-electric and audio-magnetotelluric investigations, Kingdom of Saudi Arabia: Available from SAudi Arabian Deputy Ministry for Mineral Resources Data File USGS-DF-5-46.

APPENDIX

Explanation

In the following, a computer printout of the AMT sounding data obtained from this study is presented together with log-log plots of the resistivity distribution as a function of depth. These plots were derived from the inversion algorithm discussed by Flanigan and Zablocki (1984). It is from these plots and the previously published data for AMT stations F-1 through F-15 that the geoelectric cross sections presented in this report were constructed. Note that measurements for station CMOT-5 were made only in the east-west direction.

STA. ID_SG01 NS NO FREQ= 12

FREQ	AP-RES	N OBS	D ERR
7.512	845.00	10	1292.80
14.012	563.00	10	842.29
27.010	688.00	11	864.22
45.010	239.00	13	715.39
75.0	8201.80	12	787.14
140.0	4542.60	12	565.33
270.0	5371.80	14	408.84
450.0	3858.70	11	252.40
750.0	3621.20	16	176.99
4500.0	1739.50	15	63.96
7500.0	764.94	12	47.23
14000.0	314.17	9	45.09

STA. ID_SG01 EW NO FREQ= 13

FREQ	AP-RES	N OBS	STD ERR
4.5	2352.10	6	1035.70
7.5	3868.80	12	437.18
14.0	2783.70	12	304.84
27.0	3200.90	10	417.22
45.0	1921.00	11	270 .5
75.0	?276.70	11	252 7
140.0	1973.40	10	409.20
270.0	2296.60	10	424.09
450.0	968.81	8	804.73
1400.0	304.53	5	28.10
4500.0	329.64	12	141.24
7500.0	522.35	12	145.76
14000.0	174.81	10	13.25

STA. ID_SG05 NS NO FREQ= 12

FREQ	AP-RES	N OBS	STD ERR
4.5	273.83	8	76.69
7.5	469.31	10	55.99
14.0	591.90	10	34.45
27.0	611.73	11	48.45
45.0	419.79	10	22.94
75.0	433.02	12	21.98
140.0	192.03	12	9.04
270.0	229.73	12	10.02
450.0	167.20	10	5.81
1400.0	43.58	3	20.34
4500.0	43.04	10	2.52
7500.0	21.06	11	2.02

STA. ID_SG05 EW NO FREQ= 13

FREQ	AP-RES	N OBS	STD ERR
4.5	1022.10	8	230.60
7.5	1488.20	15	91.31
14.0	1021.90	14	44.83
27.0	713.19	12	39.26
45.0	531.19	11	30.52
75.0	319.49	10	20.28
140.0	317.16	15	18.11
270.0	188.09	12	15.45
450.0	91.48	11	7.61
750.0	61.30	10	5.94
4500.0	32.37	11	2.67
7500.0	19.96	11	1.25
14000.0	17.69	10	.27

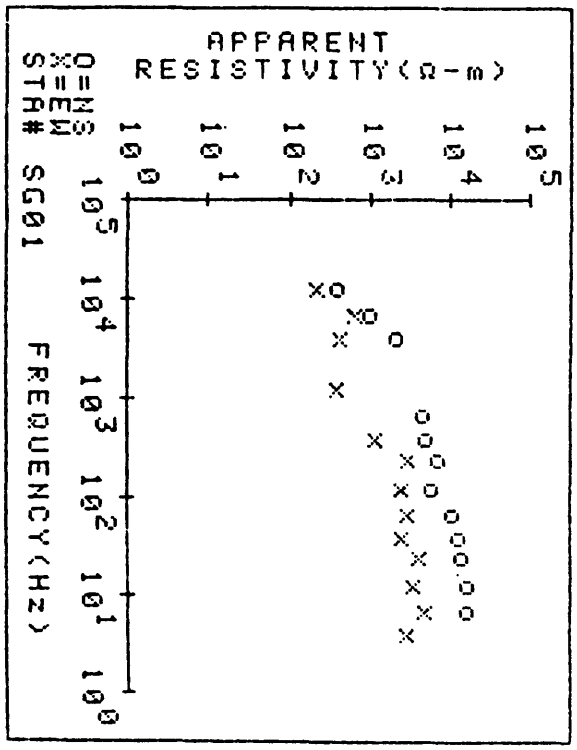

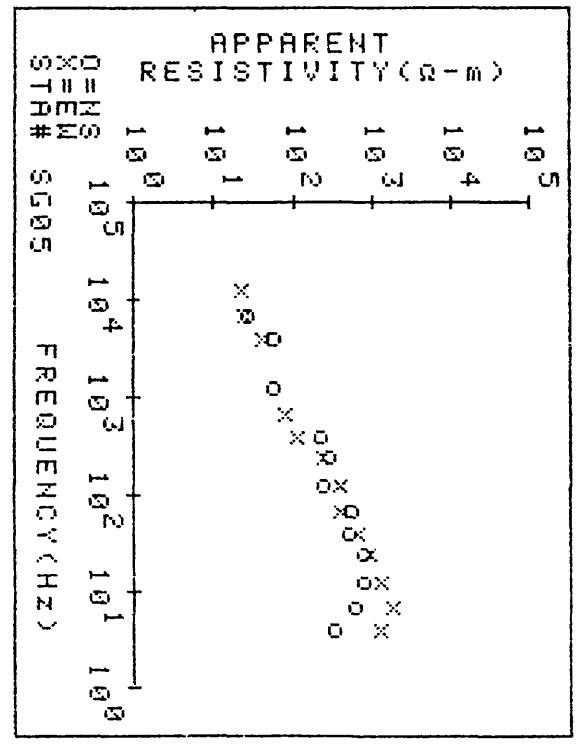

STA. ID_SG09 NS NO FREQ= 13

FREQ	AP-RES	N OBS	STD ERR
4.520	409.00	5	2215.30
7.527	682.00	12	2990.20
14.025	353.00	12	2179.60
27.015	081.00	13	2091.30
45.0	9168.60	11	1134.30
75.0	9302.60	10	690.95
140.0	4539.10	14	233.79
270.0	5211.50	12	371.29
450.0	4240.20	10	128.79
750.0	2887.80	12	119.22
2700.0	351.45	2	60.14
14000.0	361.45	10	47.71
27000.0	159.19	10	14.79

STA. ID_SG09 EW NO FREQ= 12

FREQ	AP-RES	N OBS	STD ERR
4.5	5860.50	8	1057.00
7.5	4081.90	11	232.09
14.0	4421.20	13	161.33
27.0	2916.30	13	152.34
45.0	2279.80	11	190.19
75.0	2470.00	14	183.54
140.0	1783.30	14	182.11
270.0	832.40	12	198.01
2700.0	259.95	5	55.69
7500.0	60.32	12	10.18
14000.0	45.59	12	6.19
27000.0	22.69	10	1.98

STA. ID_SG013 NS NO FREQ= 11

FREQ	AP-RES	N OBS	STD ERR
7.5	3666.60	12	329.10
14.0	2575.40	11	162.87
27.0	1724.60	12	102.03
45.0	903.24	12	69.38
75.0	671.21	14	51.66
140.0	237.50	13	22.19
270.0	293.95	14	18.73
450.0	234.25	15	7.64
4500.0	17.42	11	.76
7500.0	8.99	15	.55
14000.0	8.42	10	.96

STA. ID_SG013 EW NO FREQ= 13

FREQ	AP-RES	N OBS	STD ERR
7.5	1268.10	12	138.58
14.0	761.26	14	143.91
27.0	581.31	10	40.74
45.0	555.47	12	59.05
75.0	550.89	15	40.91
140.0	432.70	13	25.14
270.0	285.36	14	14.52
450.0	187.33	10	12.96
750.0	108.96	17	7.00
4500.0	13.17	11	.77
7500.0	12.50	15	.57
14000.0	9.69	13	.34
27000.0	8.36	10	1.07

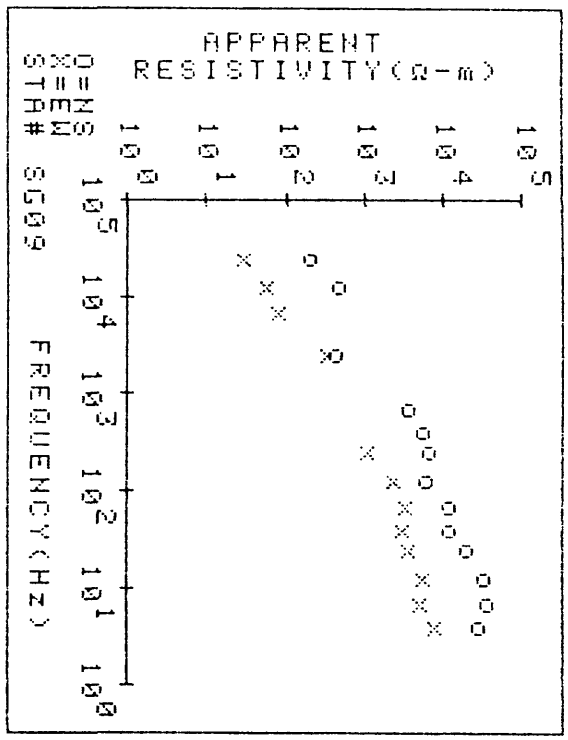

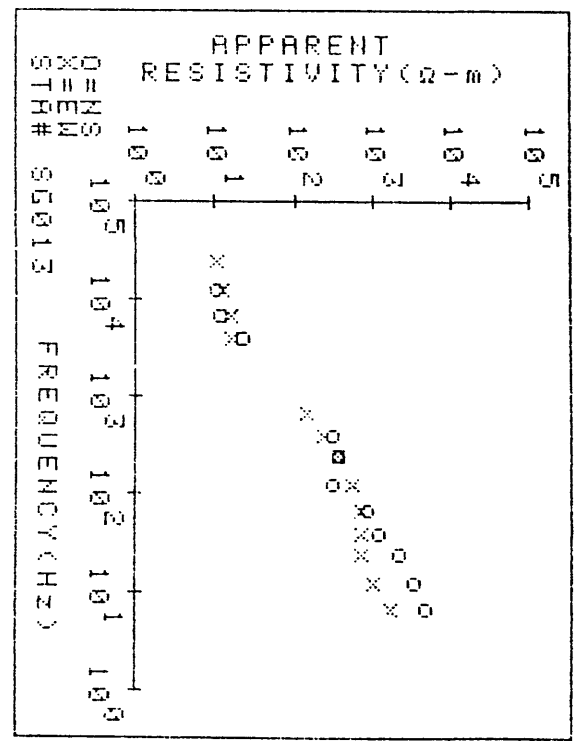

STA. ID_SG17 NS NO FREQ= 10

FREQ	AP-RES	N OBS	STD ERR
4.5	420.26	9	79.66
7.5	654.74	12	67.98
14.0	540.73	11	22.66
27.0	299.86	13	12.43
45.0	170.45	11	8.25
75.0	131.31	10	15.06
140.0	47.73	18	2.73
450.0	88.39	10	62.56
7500.0	11.79	12	.71
27000.0	19.44	7	1.81

STA. ID_SG17 EW NO FREQ= 11

FREQ	AP-RES	N OBS	STD ERR
4.5	215.03	10	65.66
7.5	222.29	12	16.27
14.0	152.28	10	15.24
27.0	170.83	10	10.80
45.0	126.78	12	7.07
75.0	102.66	11	8.78
140.0	91.66	12	6.50
450.0	61.83	7	10.04
750.0	86.86	5	24.35
7500.0	8.98	10	.59
14000.0	8.74	12	.54

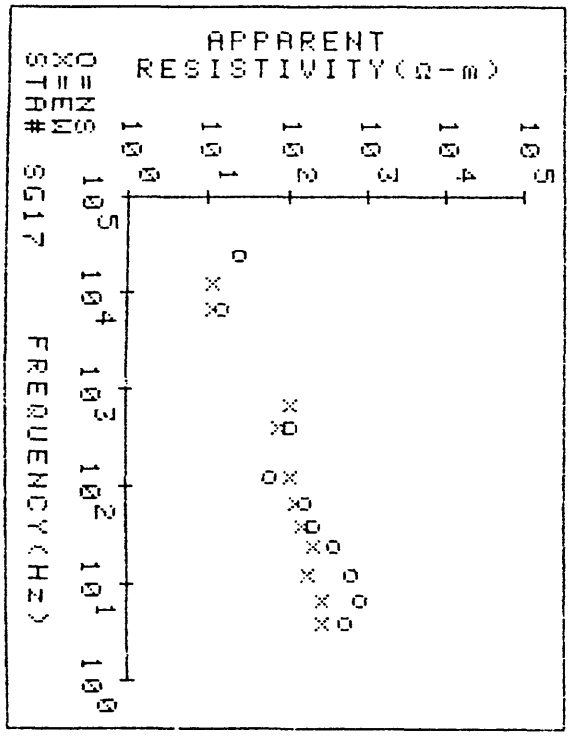

STA. ID_CMOT01 NS NO FREQ= 12

FREQ	AP-RES	N OBS	STD ERR
4.519869.00		5	2325.50
7.521152.00		10	1719.90
27.022181.00		11	5215.90
45.016634.00		11	2581.90
75.011975.00		14	1299.70
140.0	4920.60	10	735.29
270.0	7560.30	11	1254.40
450.0	4653.90	12	1136.90
750.0	5245.60	9	1218.10
4500.0	6997.60	11	2233.80
7500.0	4408.70	18	361.05
14000.0	1617.30	10	357.58

STA. ID_CMOT01 EW NO FREQ= 13

FREQ	AP-RES	N OBS	STD ERR
4.5	3168.80	8	642.70
7.5	4956.50	10	572.66
14.0	6519.80	9	447.16
27.0	5725.50	10	540.05
45.0	6123.80	10	743.01
75.0	5995.80	12	2428.00
140.0	5226.40	10	685.16
270.0	3426.80	10	814.83
450.0	2365.70	11	345.60
750.0	2864.10	4	432.24
4500.0	2243.10	11	579.41
7500.0	1664.00	10	172.60
14000.0	3632.90	11	459.55

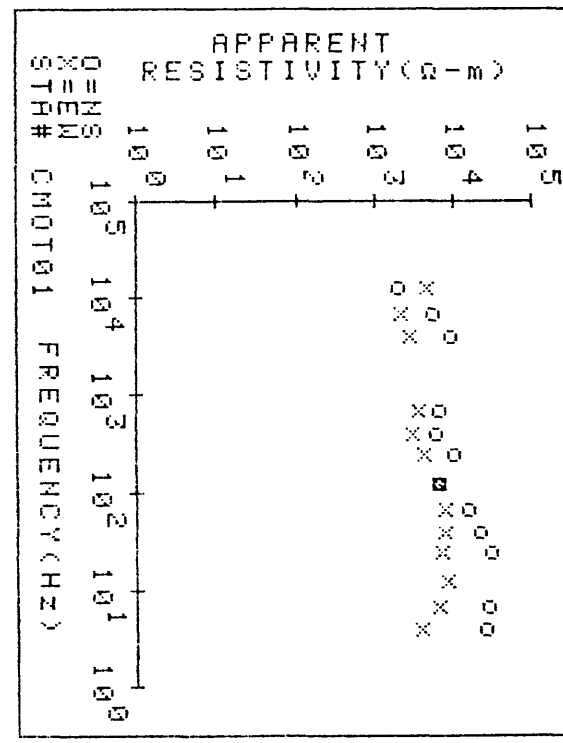

STA. ID_CMOT02 NS NO FREQ= 11

FREQ	AP-RES	N OBS	STD ERR
4.5	7350.90	7	1391.40
7.5	10928.00	8	4832.40
14.0	9844.60	9	1223.30
27.0	7485.80	12	949.15
45.0	4284.20	10	670.84
75.0	3346.70	12	381.30
140.0	1554.50	11	166.90
270.0	1775.00	11	100.95
450.0	1289.70	12	88.16
750.0	1125.20	8	113.45
14000.0	229.25	11	13.85

STA. ID_CMOT02 EW NO FREQ= 12

FREQ	AP-RES	N OBS	STD ERR
4.5	1502.70	8	368.63
7.5	1911.00	13	303.15
14.0	1562.30	11	125.86
27.0	1954.00	12	120.87
45.0	1284.50	11	287.44
75.0	1295.40	12	121.25
140.0	1554.10	10	218.50
270.0	1269.40	11	159.75
450.0	1320.60	10	48.97
750.0	715.50	7	565.80
4500.0	534.57	10	84.85
14000.0	373.78	10	51.13

STA. ID_CMOT03 NS NO FREQ= 12

FREQ	AP-RES	N OBS	STD ERR
7.5	3840.60	10	760.63
14.0	3192.10	11	413.31
27.0	2005.40	12	292.93
45.0	1527.30	12	97.16
75.0	1169.70	10	76.59
140.0	625.00	11	42.93
270.0	750.09	13	57.98
450.0	693.85	12	26.90
750.0	699.92	11	94.96
4500.0	293.89	10	38.80
7500.0	221.24	12	14.60
14000.0	194.25	9	38.25

STA. ID_CMOT03 EW NO FREQ= 13

FREQ	AP-RES	N OBS	STD ERR
4.5	8150.40	10	1300.70
7.5	5644.90	10	772.26
14.0	4064.90	11	406.95
27.0	2604.50	12	227.65
45.0	1593.40	10	173.39
75.0	902.82	12	125.67
140.0	610.57	16	66.34
270.0	380.88	11	28.60
450.0	327.48	12	13.12
750.0	255.22	9	43.15
4500.0	140.64	14	11.29
7500.0	97.94	10	5.28
27000.0	93.13	10	37.69

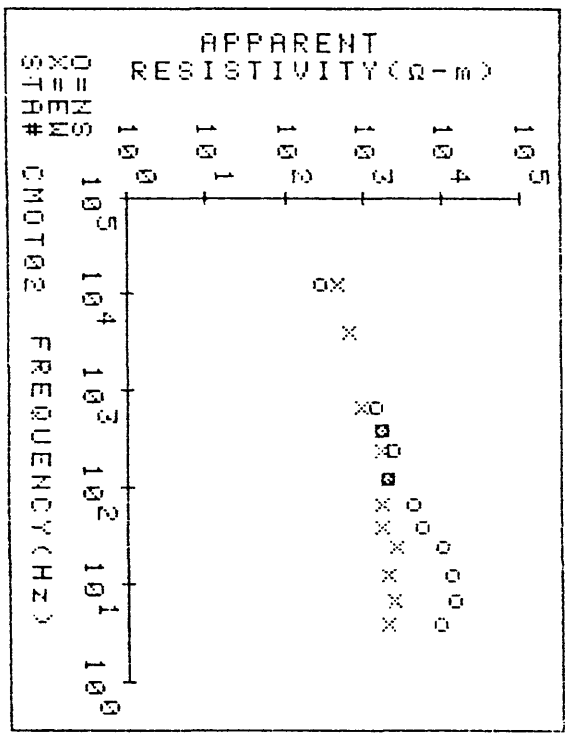

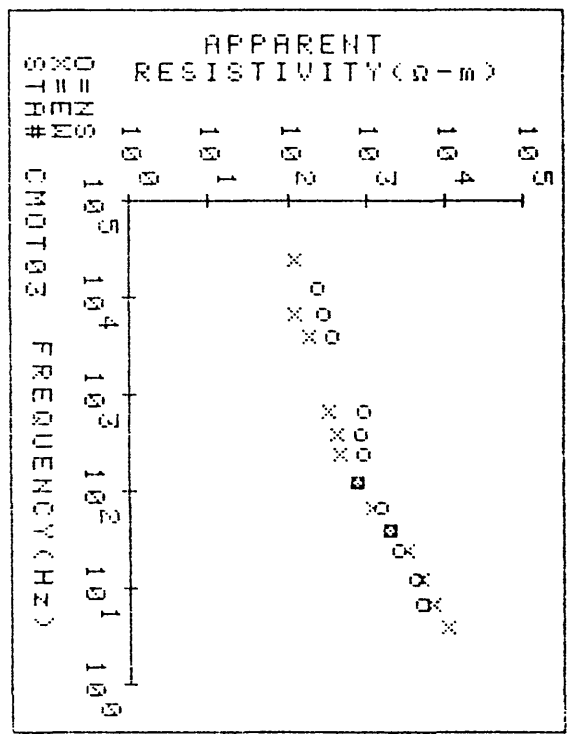

STA. ID_CMOT04 NS NO FREQ= 14

FREQ	AP-RES	N OBS	STD ERR
4.5	1362.70	10	301.10
7.5	2210.40	13	87.28
14.0	1769.30	14	86.85
27.0	1482.20	11	61.62
45.0	1114.00	13	43.58
75.0	1043.80	11	39.20
140.0	519.32	12	20.71
270.0	620.27	11	20.89
450.0	723.95	10	47.94
750.0	363.65	10	43.01
4500.0	403.69	11	58.58
7500.0	139.83	11	13.56
14000.0	60.41	12	5.27
27000.0	39.11	10	3.45

STA. ID_CMOT04 EW NO FREQ= 14

FREQ	AP-RES	N OBS	STD ERR
4.5	6475.70	10	1429.60
7.5	8142.80	13	486.48
14.0	4875.90	14	167.58
27.0	3666.20	13	158.85
45.0	2614.10	10	107.33
75.0	2137.30	12	105.88
140.0	2076.40	10	163.97
270.0	1179.30	13	123.20
450.0	768.53	13	57.83
750.0	352.47	11	61.52
4500.0	174.67	11	7.87
7500.0	84.35	10	4.93
14000.0	81.07	10	11.42
27000.0	24.62	11	4.08

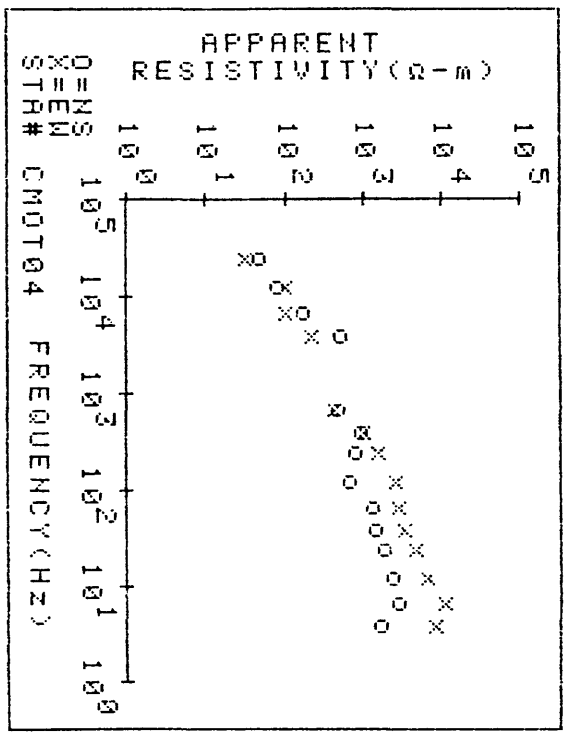

NO DATA N-S

STA. ID_CMOT05 EW NO FREQ= 14

FREQ	AP-RES	N OBS	STD ERR
4.5	382.90	9	78.30
7.5	256.08	10	97.92
14.0	109.02	10	11.45
27.0	88.51	9	10.60
45.0	69.39	10	3.26
75.0	61.94	10	7.49
140.0	86.10	10	10.79
270.0	134.91	10	9.61
450.0	106.83	10	14.39
750.0	116.22	10	17.09
4500.0	91.61	11	6.17
7500.0	44.75	10	7.35
14000.0	47.61	10	9.97
27000.0	32.39	12	2.01

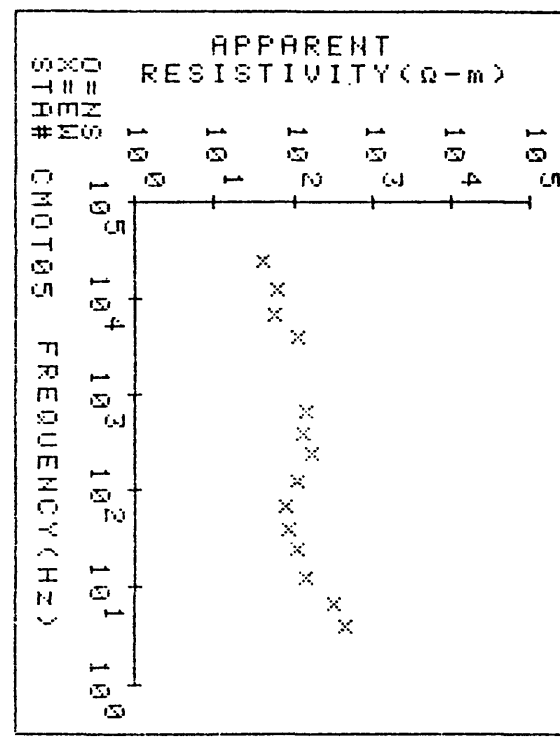

STA. ID_CMOT11 NS NO FREQ= 10

FREQ	AP-RES	N OBS	STD ERR
7.5	862.36	9	225.39
13.6	1172.90	12	198.54
27.0	642.49	10	116.86
45.0	402.06	10	39.52
75.0	293.20	10	24.96
136.0	158.61	10	53.82
270.0	67.21	11	11.05
450.0	82.39	11	26.25
7500.0	9.64	8	2.04
13600.0	15.05	8	2.08

STA. ID_CMOT11 EW NO FREQ= 12

FREQ	AP-RES	N OBS	STD ERR
4.5	1268.30	6	336.54
7.5	981.28	10	88.48
13.6	1114.30	12	74.84
27.0	971.15	16	136.73
45 0	667.27	11	40.83
75.0	396.31	11	22.78
136.0	204.10	12	18.72
270.0	172.68	12	34.42
450.0	86.42	12	1.89
750.0	52.56	11	2.68
4500.0	54.84	10	5.76
13600.0	21.97	10	4.59

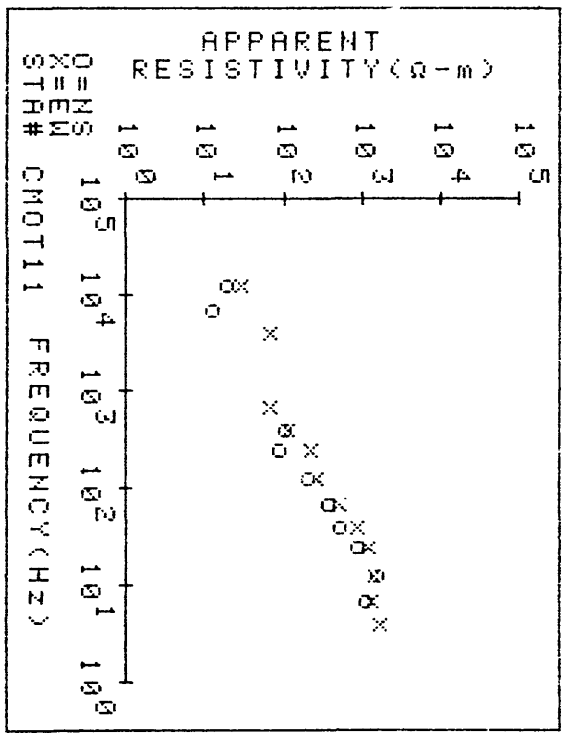

STA. ID_CMOT12 NS NO FREQ= 13

FREQ	AP-RES	N OBS	STD ERR
4.5	6681.70	10	976.40
7.5	7301.00	11	692.26
13.6	6887.90	10	478.43
27.0	4503.50	11	325.84
45.0	3909.00	11	253.28
75.0	3135.80	11	281.48
136.0	1391.50	10	57.75
270.0	981.06	11	66.63
450.0	910.09	10	78.08
750.0	1040.50	10	364.49
4500.0	2134.10	10	153.58
7500.0	1714.10	12	149.17
13600.0	1803.40	13	415.25

STA ID_CMOT12 EW NO FREQ= 11

FREQ	AP-RES	N OBS	STD ERR
7.5	8844.60	10	1146.90
13.6	8168.20	10	1233.70
27.0	7530.00	13	983.07
45.0	5733.90	11	573.12
75.0	3219.70	12	316.22
136.0	2631.40	12	303.34
270.0	1735.30	13	112.03
450.0	1426.20	12	221.37
750.0	3722.80	11	344.92
4500.0	2653.20	13	359.49
13600.0	1931.60	9	282.21

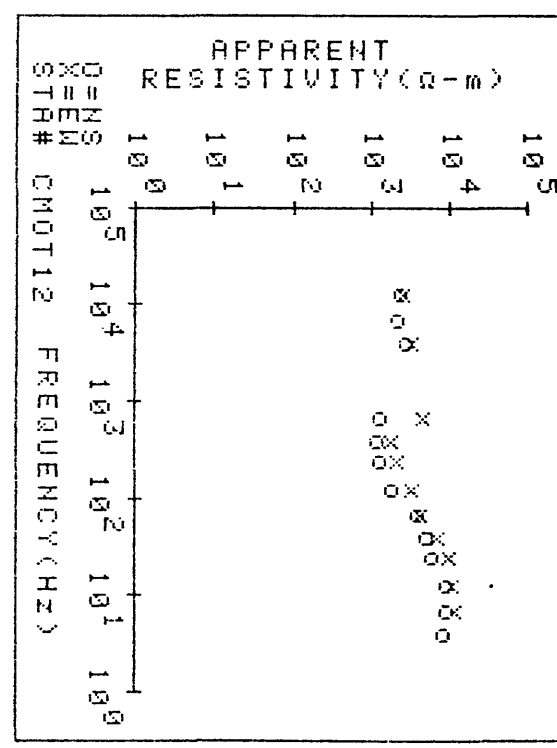

STA. ID_CMOT14 NS NO FREQ= 9

FREQ	AP-RES	N OBS	STD ERR
7.5	15.38	5	4.09
13.6	8.98	12	.78
27.0	9.25	10	.83
45.0	9.89	10	.45
75.0	11.80	11	.39
136.0	8.81	11	.20
270.0	16.69	10	.84
450.0	25.41	12	1.01
750.0	63.13	12	17.62

STA. ID_CMOT14 EW NO FREQ= 11

FREQ	AP-RES	N OBS	STD ERR
7.5	25.24	9	3.91
13.6	30.67	13	2.11
27.0	43.91	11	5.10
45.0	45.95	10	1.85
75.0	64.40	10	1.60
136.0	83.74	9	3.79
270.0	98.91	11	7.07
450.0	110.39	10	10.21
750.0	185.63	9	27.90
7500.0	108.36	12	19.65
13600.0	122.75	8	4.13

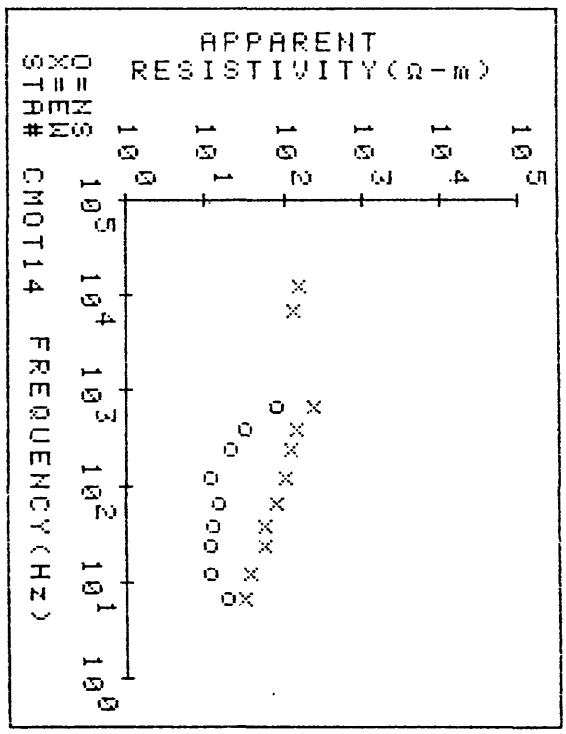

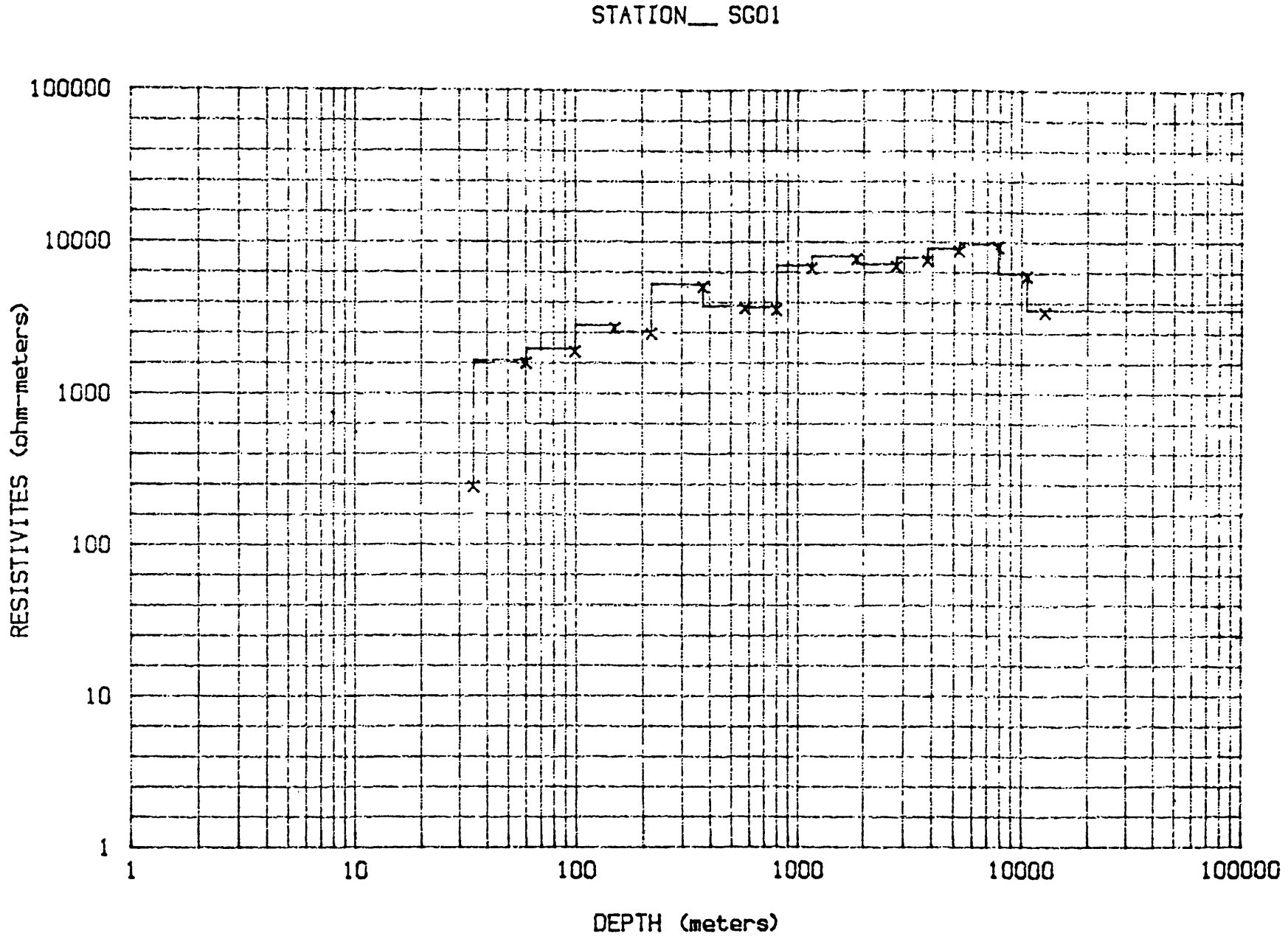
STATION__ SG01
100000
10000
1000
100
10
1
RESISTIVITES (ohm-meters)
1
10
100
1000
10000
100000
DEPTH (meters)

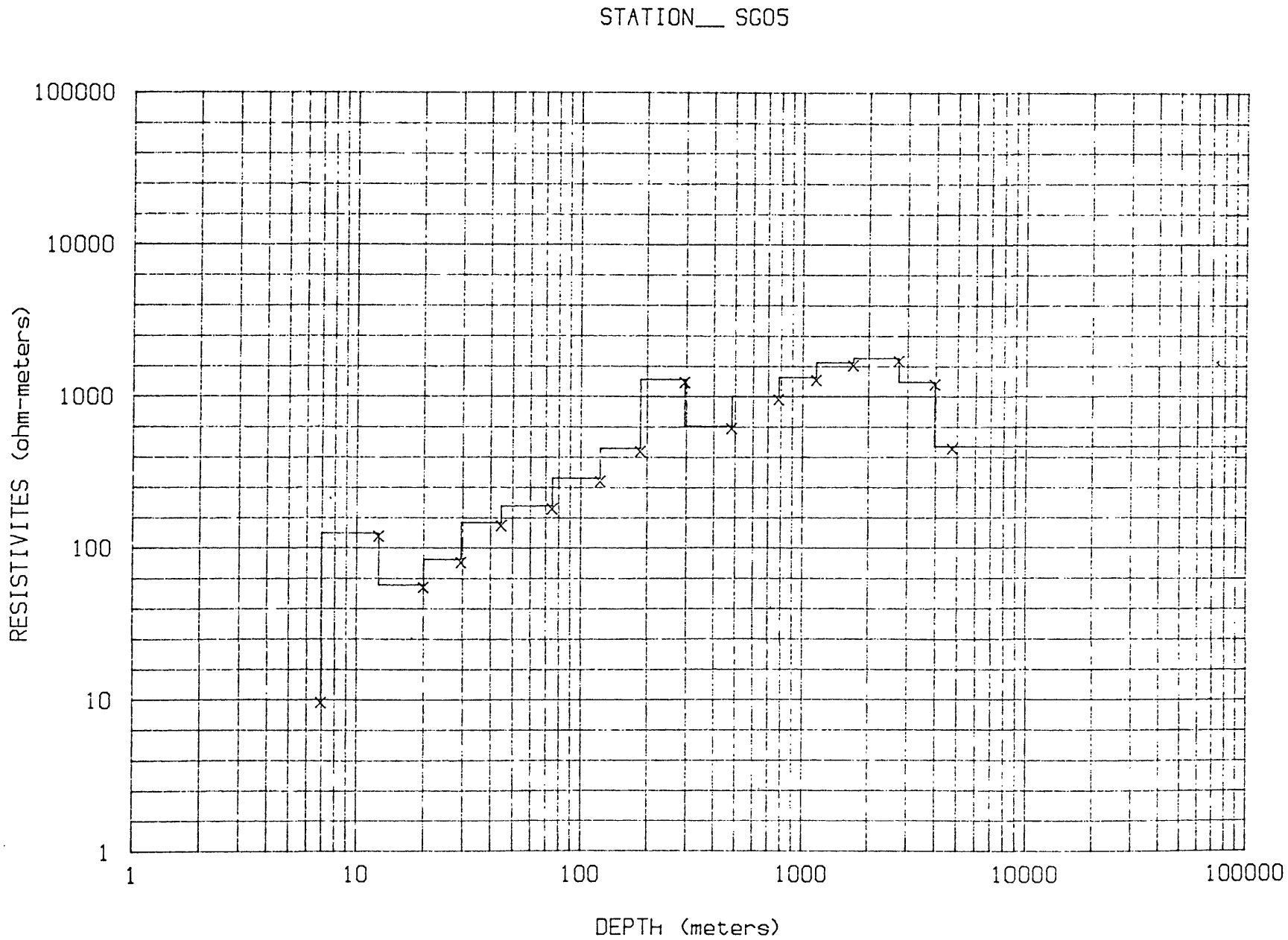
STATION__ SG05
100000
10000
1000
100
10
1
RESISTIVITES (ohm-meters)
1
10
100
1000
10000
100000
DEPTH (meters)

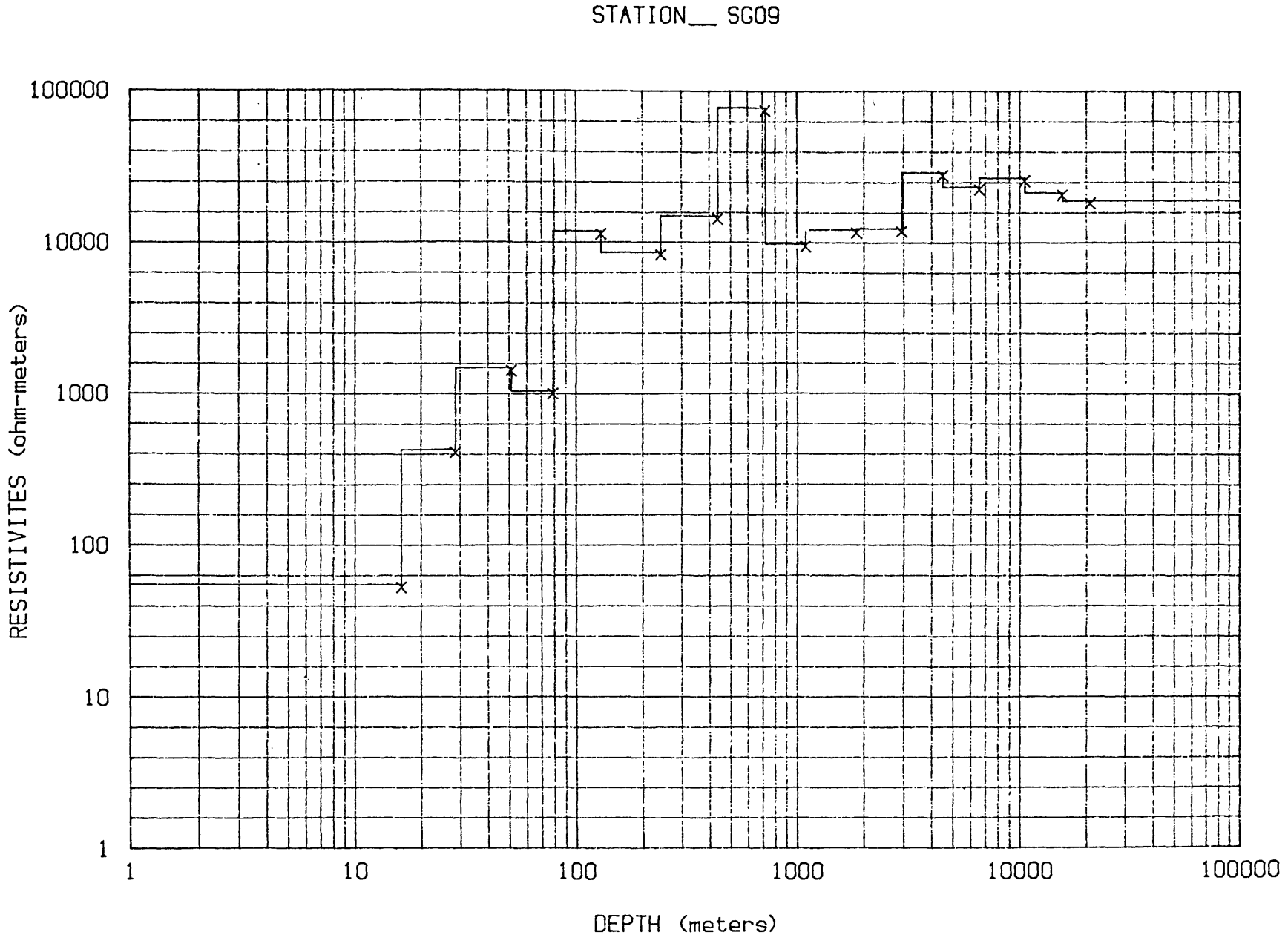
STATION__ SG09
100000
10000
1000
100
10
1
RESISTIVITES (ohm-meters)
1
10
100
1000
10000
100000
DEPTH (meters)

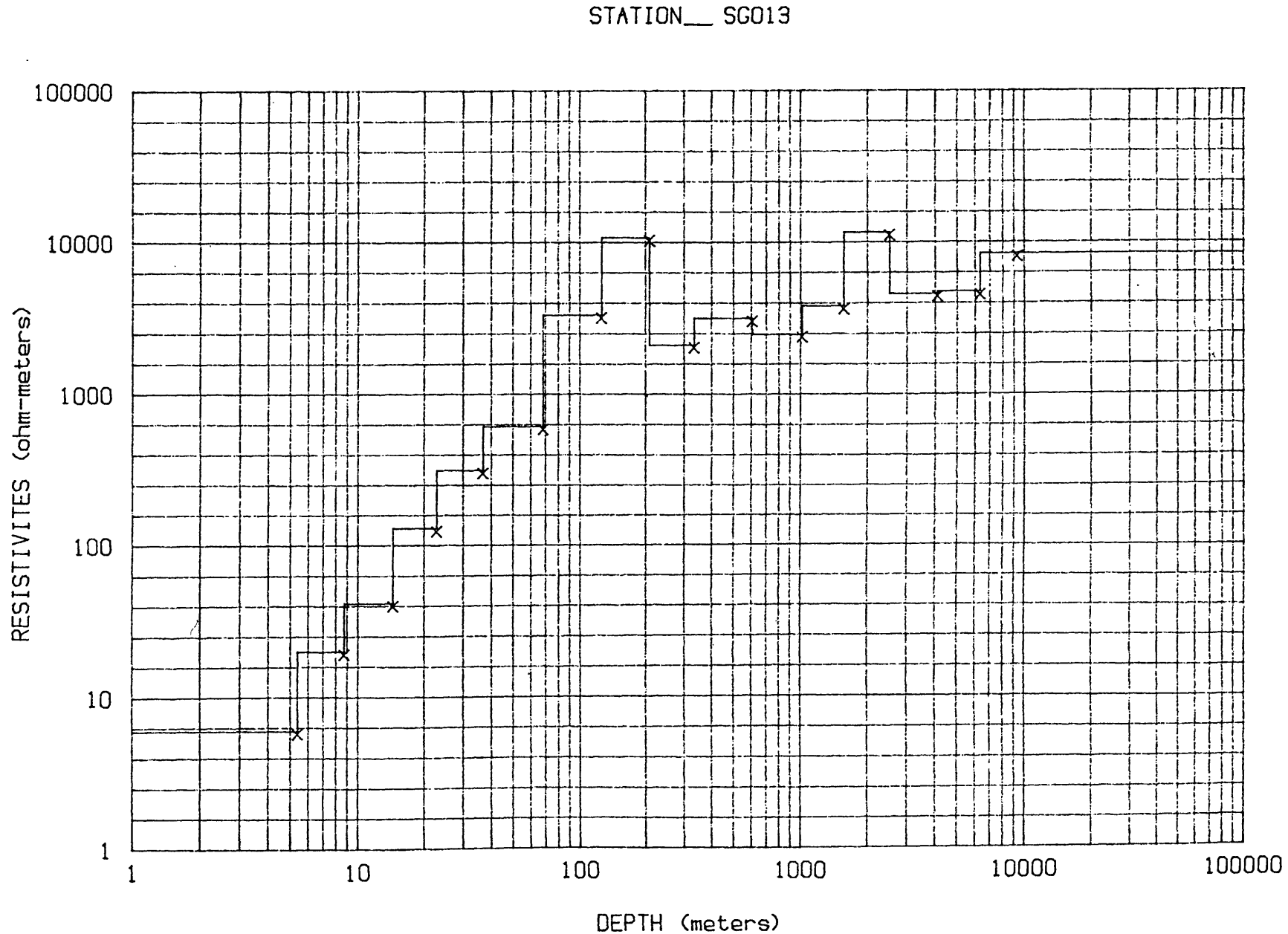
STATION__ SG013
100000
10000
1000
100
10
1
RESISTIVITES (ohm-meters)
1
10
100
1000
10000
100000
DEPTH (meters)

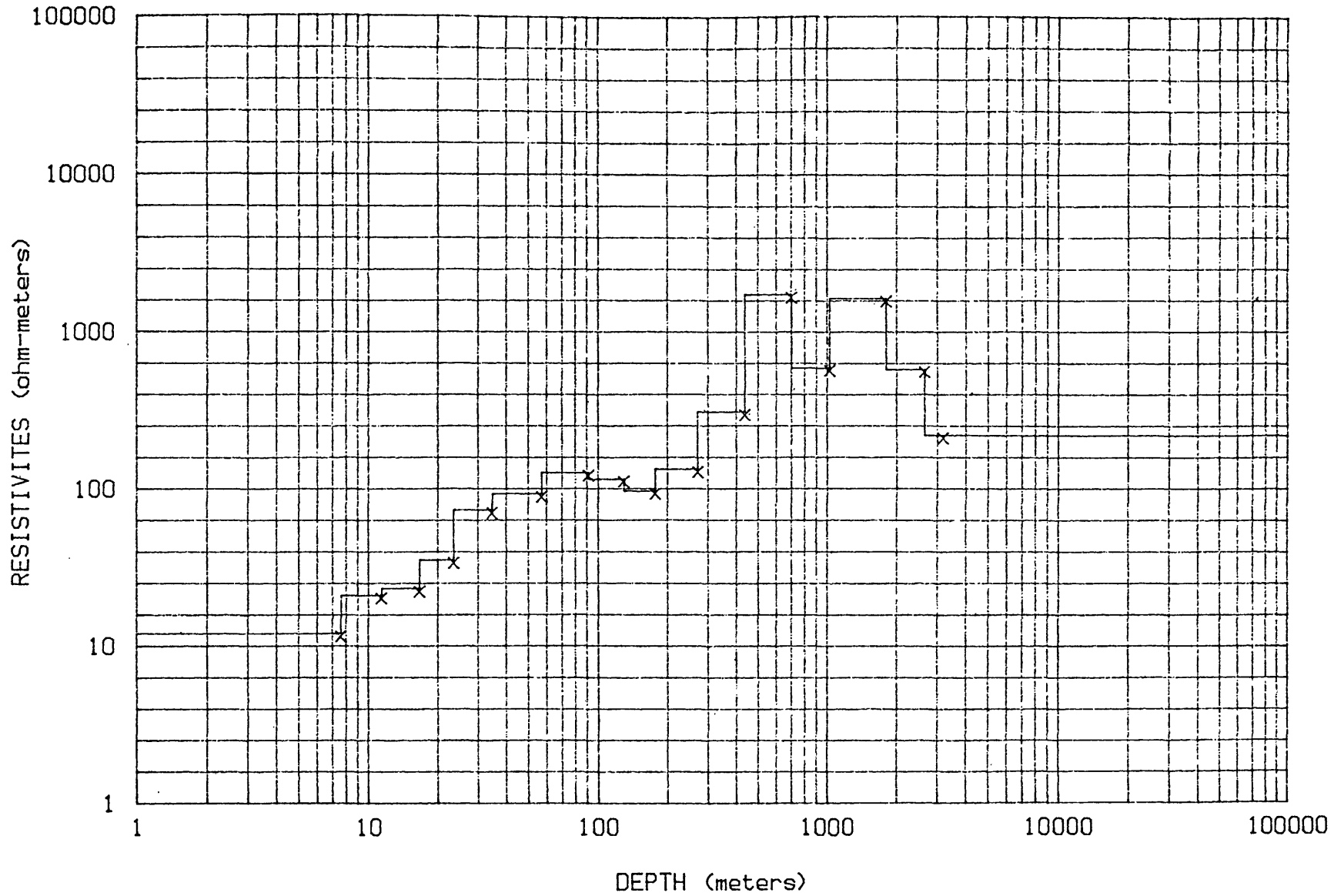
STATION__ SG17
100000
10000
1000
100
10
1
RESISTIVITES (ohm-meters)
1
10
100
1000
10000
100000
DEPTH (meters)

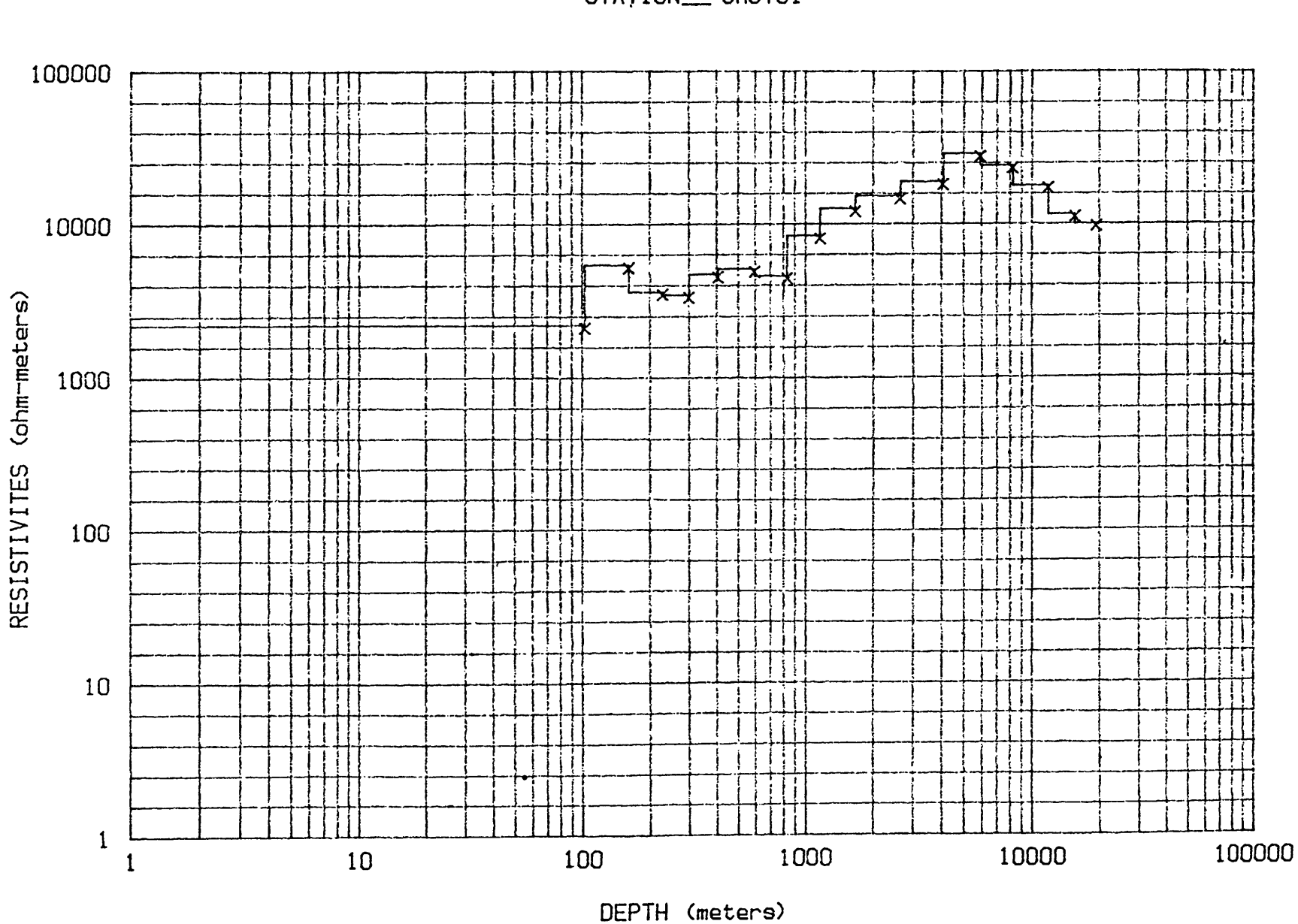
STATION__ CMOTO1
100000
10000
1000
100
10
1
RESISTIVITES (ohm-meters)
1
10
100
1000
10000
100000
DEPTH (meters)

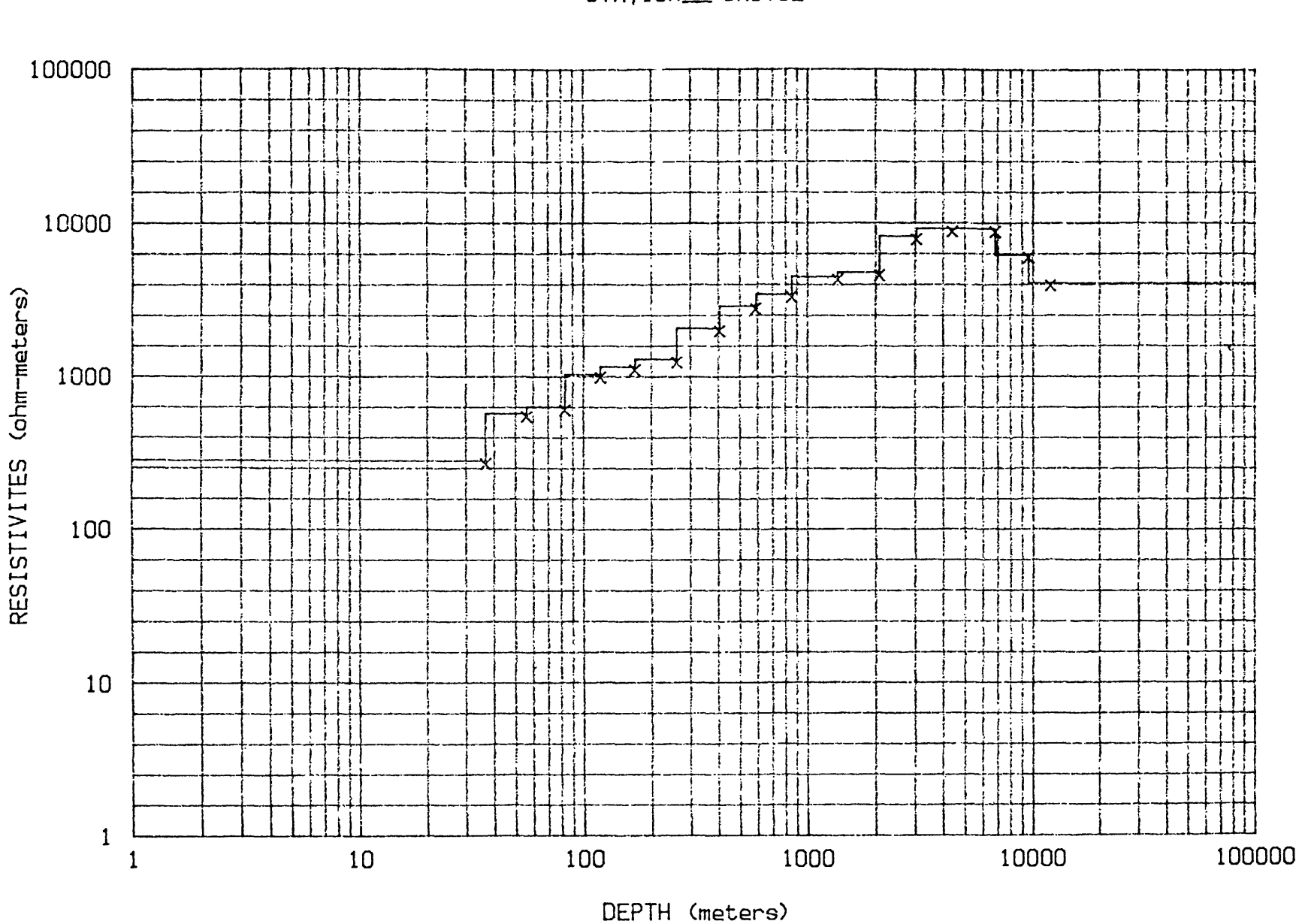
STATION__ CMOT02
100000
10000
1000
100
10
1
RESISTIVITES (ohm-meters)
1
10
100
1000
10000
100000
DEPTH (meters)

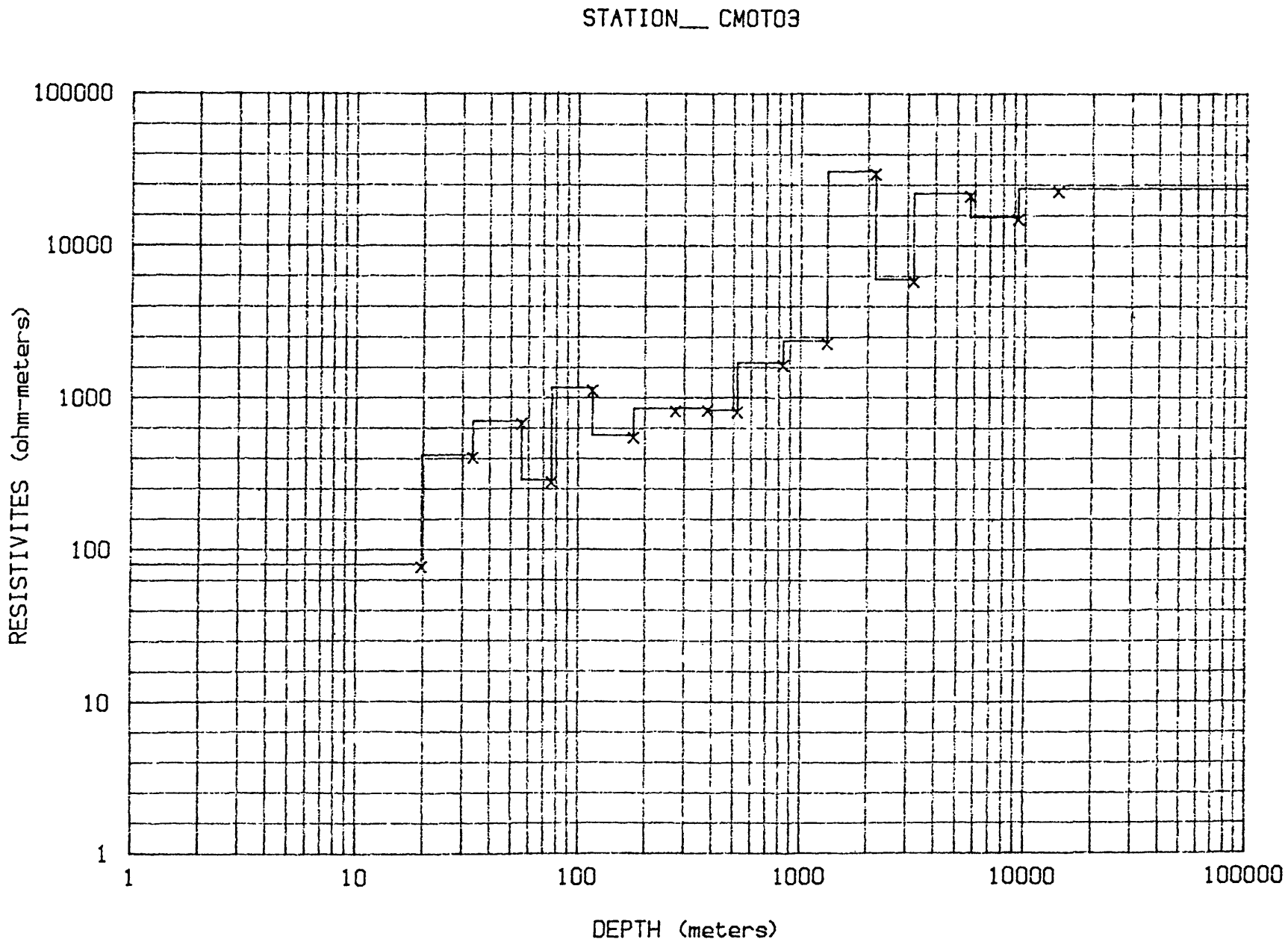
STATION__ CMOT03
100000
10000
1000
100
10
1
RESISTIVITES (ohm-meters)
1
10
100
1000
10000
100000
DEPTH (meters)

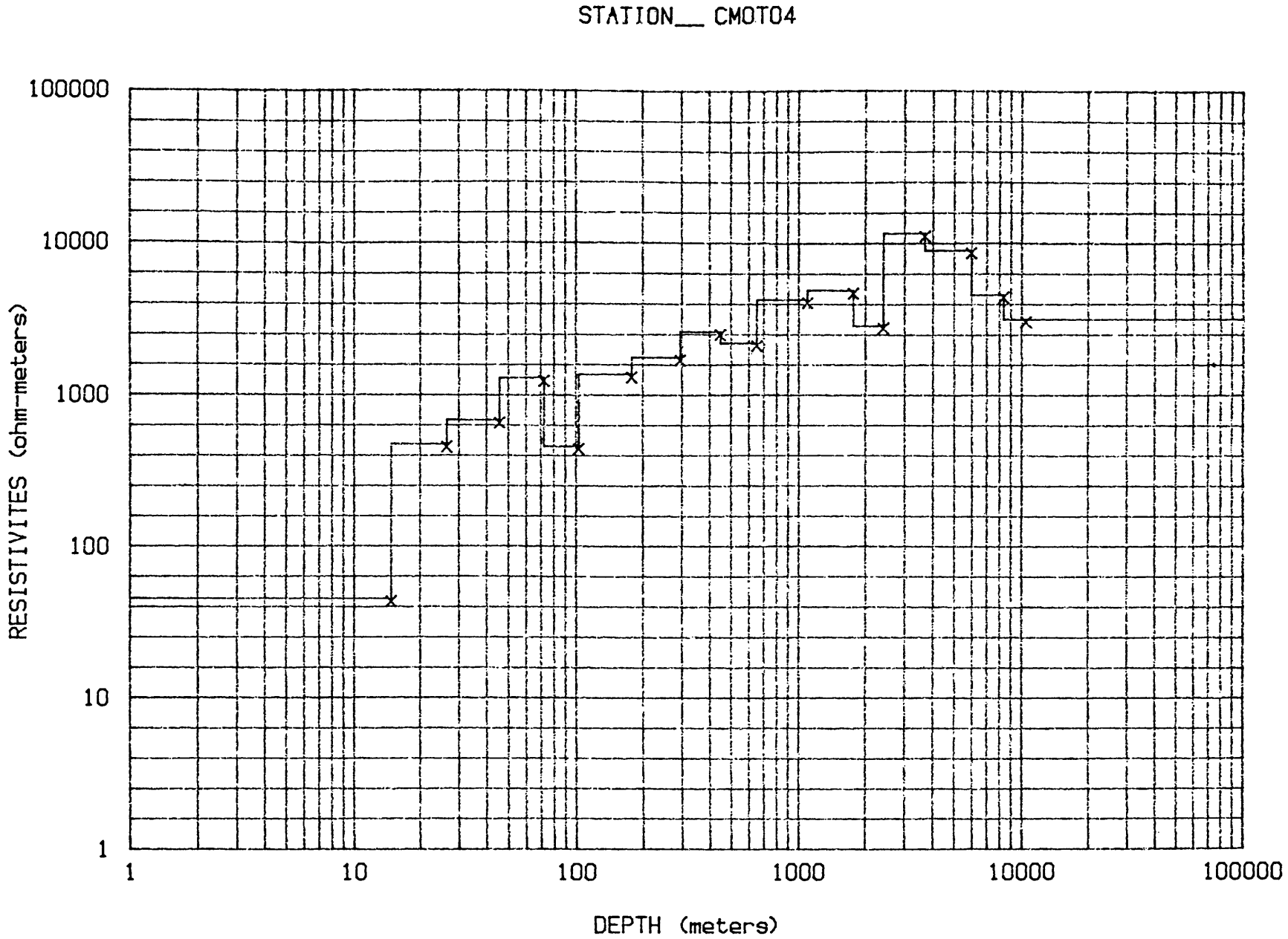
STATION__ CMOT04
100000
10000
1000
100
10
1
RESISTIVITES (ohm-meters)
1
10
100
1000
10000
100000
DEPTH (meters)

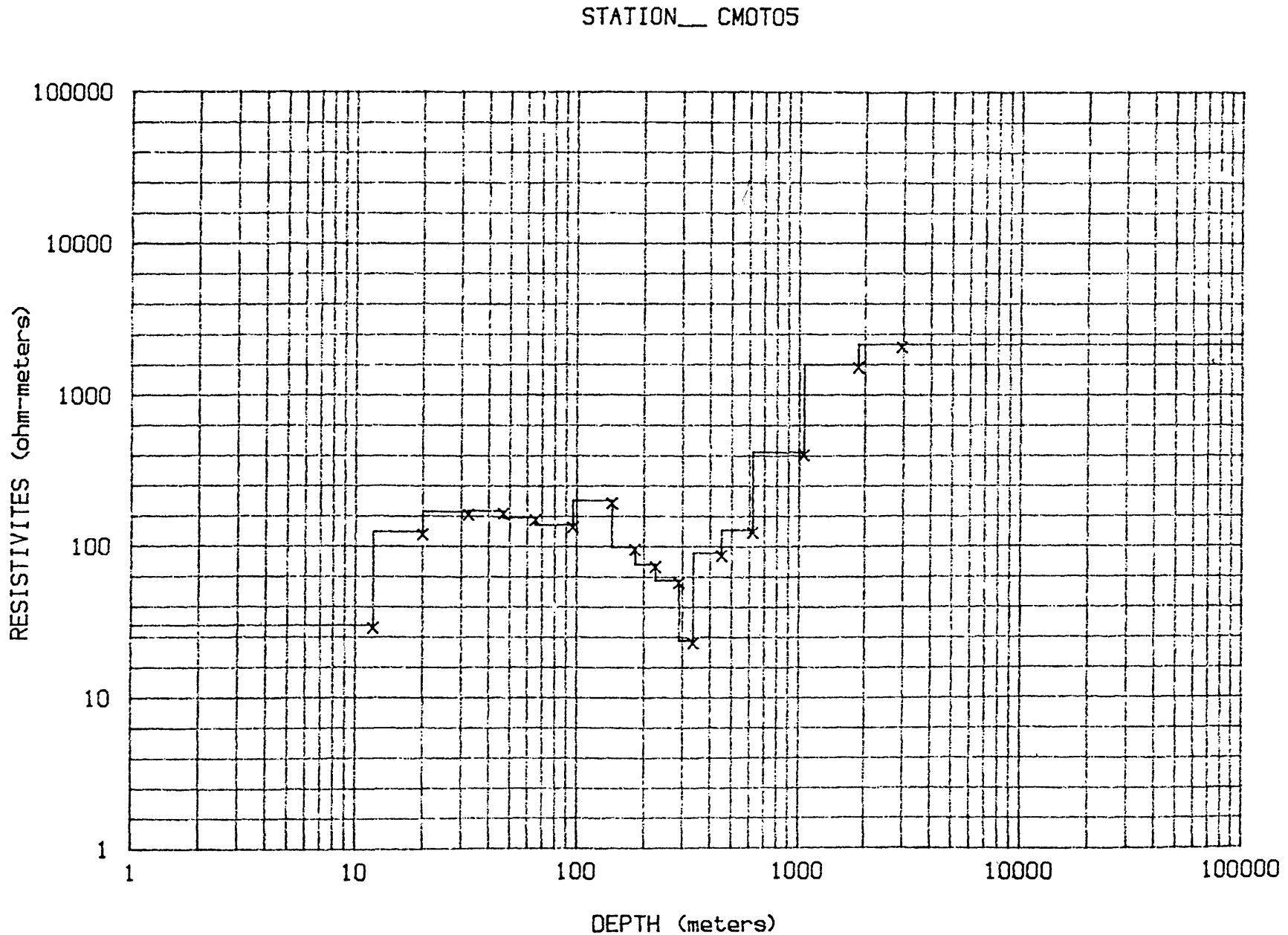
STATION__ CMOT05
100000
10000
1000
100
10
1
RESISTIVITES (ohm-meters)
1
10
100
1000
10000
100000
DEPTH (meters)

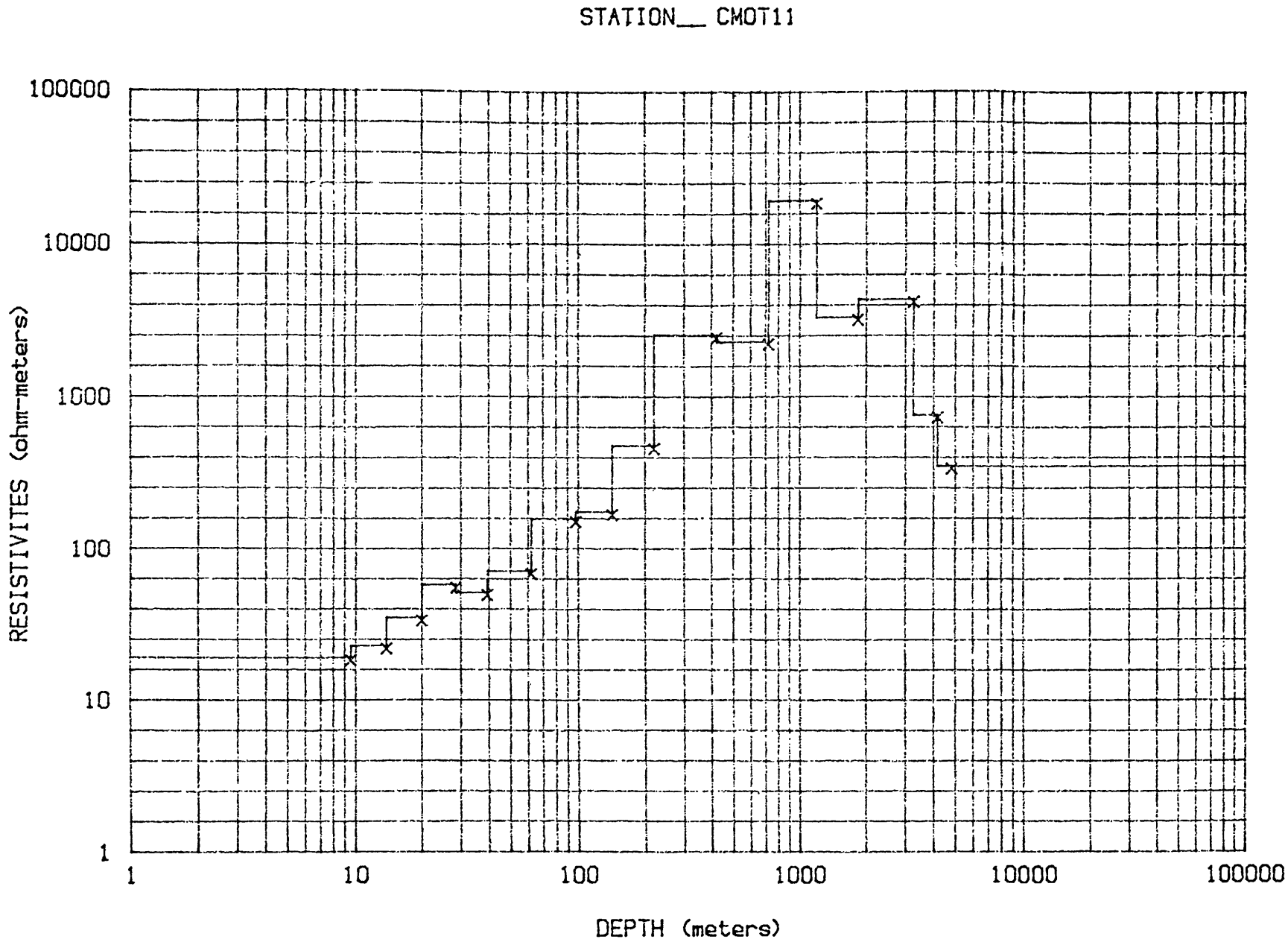
STATION__ CMOT11
100000
10000
1000
100
10
1
RESISTIVITES (ohm-meters)
1
10
100
1000
10000
100000
DEPTH (meters)

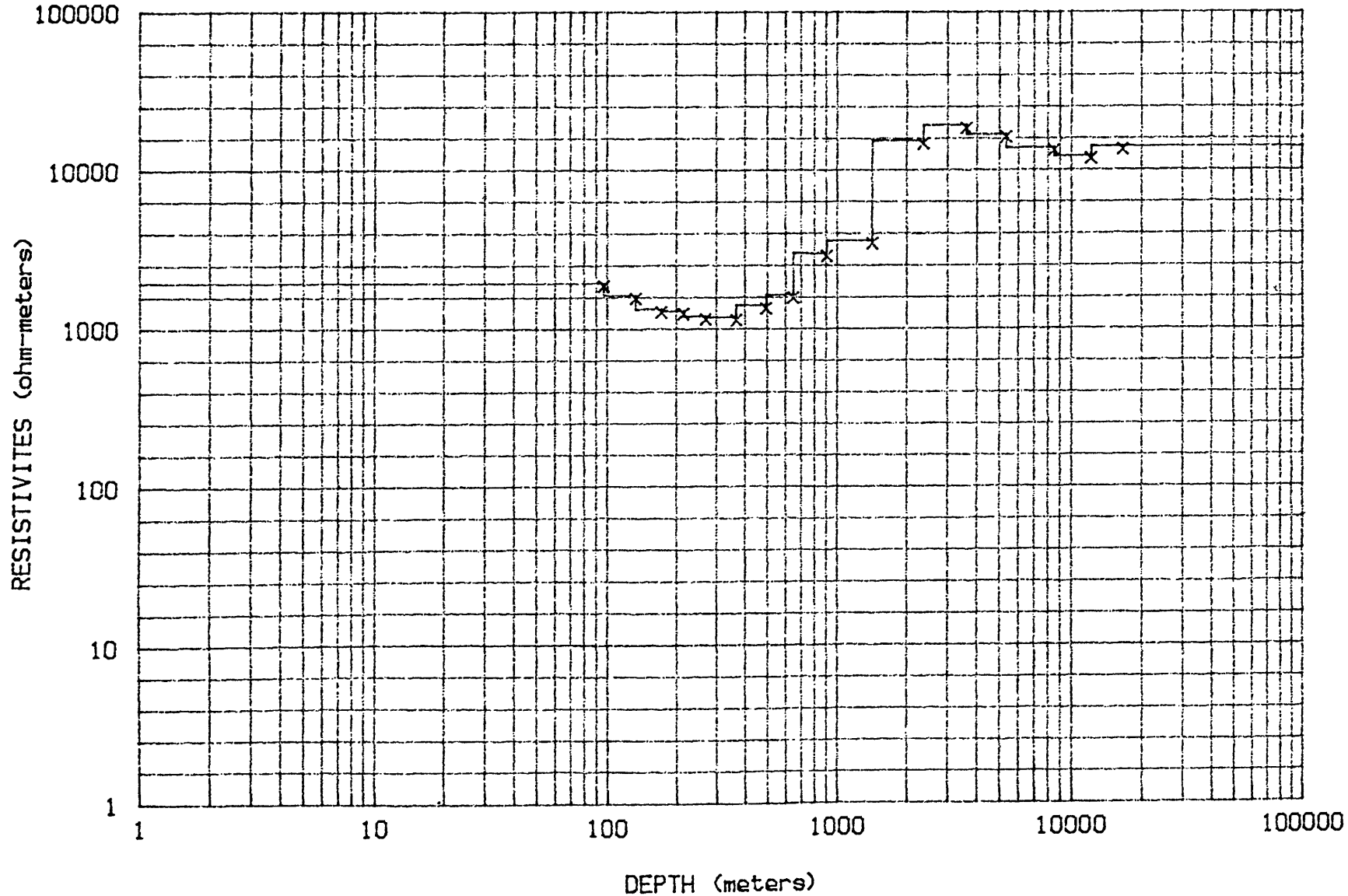
STATION__ CMOT12
100000
10000
1000
100
10
1
RESISTIVITES (ohm-meters)
1
10
100
1000
10000
100000
DEPTH (meters)

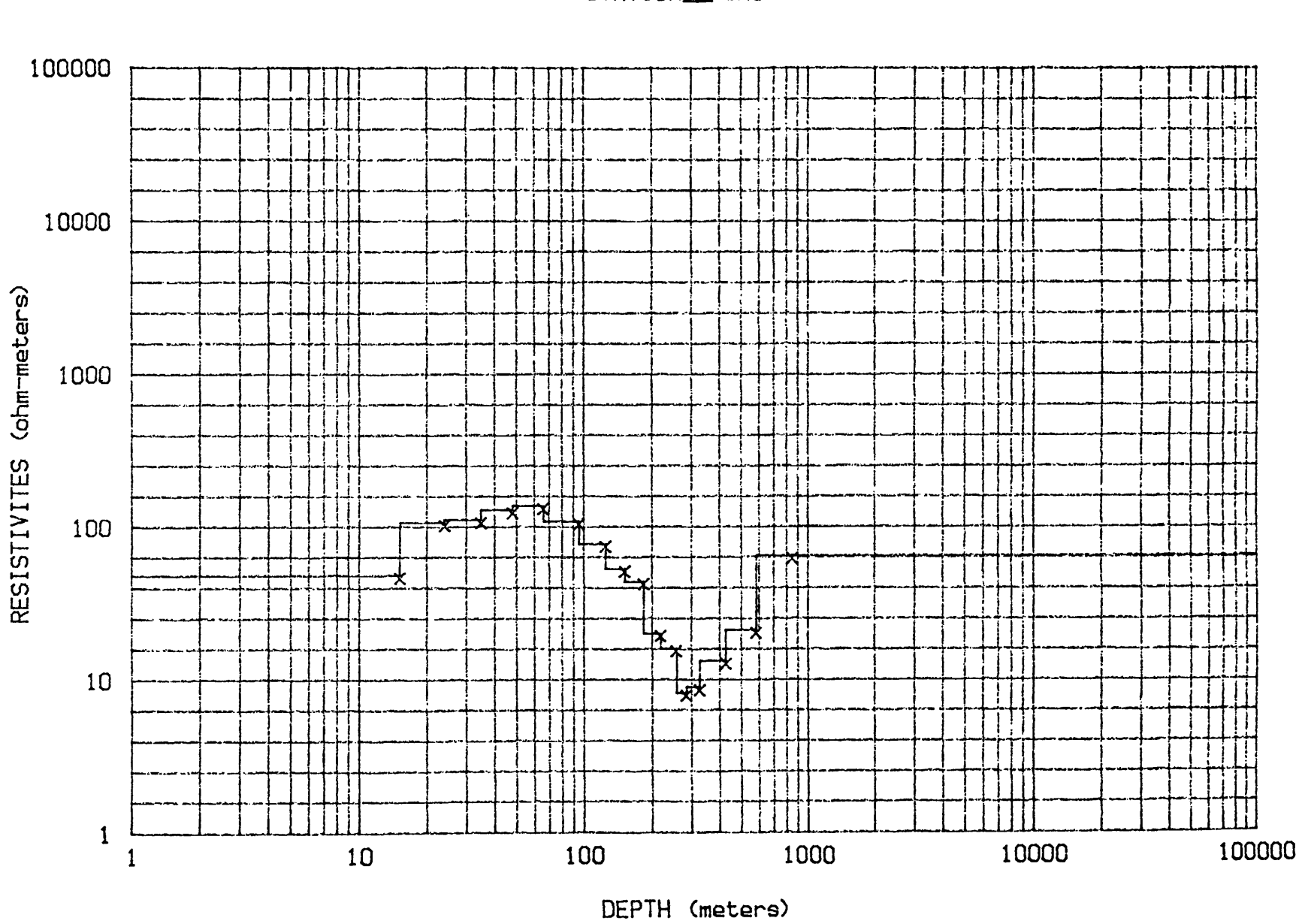
STATION__ CMOT14
100000
10000
1000
100
10
1
RESISTIVITES (ohm-meters)
1
10
100
1000
10000
100000
DEPTH (meters)